International Journal of Physical Sciences

Volume 10 Number 9 16 May, 2015

ISSN 1992-1950

Academic Journals

ABOUT IJPS

The **International Journal of Physical Sciences (IJPS)** is published weekly (one volume per year) by Academic Journals.

International Journal of Physical Sciences (IJPS) is an open access journal that publishes high-quality solicited and unsolicited articles, in English, in all Physics and chemistry including artificial intelligence, neural processing, nuclear and particle physics, geophysics, physics in medicine and biology, plasma physics, semiconductor science and technology, wireless and optical communications, materials science, energy and fuels, environmental science and technology, combinatorial chemistry, natural products, molecular therapeutics, geochemistry, cement and concrete research, metallurgy, crystallography and computer-aided materials design. All articles published in IJPS are peer-reviewed.

Contact Us

Editorial Office: ijps@academicjournals.org

Help Desk: helpdesk@academicjournals.org

Website: http://www.academicjournals.org/journal/IJPS

Submit manuscript online http://ms.academicjournals.me/

Editors

Prof. Sanjay Misra
Department of Computer Engineering, School of Information and Communication Technology
Federal University of Technology, Minna,
Nigeria.

Prof. Songjun Li
School of Materials Science and Engineering,
Jiangsu University,
Zhenjiang,
China

Dr. G. Suresh Kumar
Senior Scientist and Head Biophysical Chemistry
Division Indian Institute of Chemical Biology
(IICB)(CSIR, Govt. of India),
Kolkata 700 032,
INDIA.

Dr. 'Remi Adewumi Oluyinka
Senior Lecturer,
School of Computer Science
Westville Campus
University of KwaZulu-Natal
Private Bag X54001
Durban 4000
South Africa.

Prof. Hyo Choi
Graduate School
Gangneung-Wonju National University
Gangneung,
Gangwondo 210-702, Korea

Prof. Kui Yu Zhang
Laboratoire de Microscopies et d'Etude de Nanostructures (LMEN)
Département de Physique, Université de Reims,
B.P. 1039. 51687,
Reims cedex,
France.

Prof. R. Vittal
Research Professor,
Department of Chemistry and Molecular Engineering
Korea University, Seoul 136-701,
Korea.

Prof Mohamed Bououdina
Director of the Nanotechnology Centre
University of Bahrain
PO Box 32038,
Kingdom of Bahrain

Prof. Geoffrey Mitchell
School of Mathematics,
Meteorology and Physics
Centre for Advanced Microscopy
University of Reading Whiteknights,
Reading RG6 6AF
United Kingdom.

Prof. Xiao-Li Yang
School of Civil Engineering,
Central South University,
Hunan 410075,
China

Dr. Sushil Kumar
Geophysics Group,
Wadia Institute of Himalayan Geology,
P.B. No. 74 Dehra Dun - 248001(UC)
India.

Prof. Suleyman KORKUT
Duzce University
Faculty of Forestry
Department of Forest Industrial Engineeering
Beciyorukler Campus 81620
Duzce-Turkey

Prof. Nazmul Islam
Department of Basic Sciences & Humanities/Chemistry,
Techno Global-Balurghat, Mangalpur, Near District Jail P.O: Beltalapark, P.S: Balurghat, Dist.: South Dinajpur,
Pin: 733103,India.

Prof. Dr. Ismail Musirin
Centre for Electrical Power Engineering Studies (CEPES), Faculty of Electrical Engineering, Universiti Teknologi Mara,
40450 Shah Alam,
Selangor, Malaysia

Prof. Mohamed A. Amr
Nuclear Physic Department, Atomic Energy Authority
Cairo 13759,
Egypt.

Dr. Armin Shams
Artificial Intelligence Group,
Computer Science Department,
The University of Manchester.

Editorial Board

Prof. Salah M. El-Sayed
Mathematics. Department of Scientific Computing.
Faculty of Computers and Informatics,
Benha University. Benha ,
Egypt.

Dr. Rowdra Ghatak
Associate Professor
Electronics and Communication Engineering Dept.,
National Institute of Technology Durgapur
Durgapur West Bengal

Prof. Fong-Gong Wu
College of Planning and Design, National Cheng Kung University
Taiwan

Dr. Abha Mishra.
Senior Research Specialist & Affiliated Faculty.
Thailand

Dr. Madad Khan
Head
Department of Mathematics
COMSATS University of Science and Technology
Abbottabad, Pakistan

Prof. Yuan-Shyi Peter Chiu
Department of Industrial Engineering & Management
Chaoyang University of Technology
Taichung, Taiwan

Dr. M. R. Pahlavani,
Head, Department of Nuclear physics,
Mazandaran University,
Babolsar-Iran

Dr. Subir Das,
Department of Applied Mathematics,
Institute of Technology, Banaras Hindu University,
Varanasi

Dr. Anna Oleksy
Department of Chemistry
University of Gothenburg
Gothenburg,
Sweden

Prof. Gin-Rong Liu,
Center for Space and Remote Sensing Research
National Central University, Chung-Li,
Taiwan 32001

Prof. Mohammed H. T. Qari
Department of Structural geology and remote sensing
Faculty of Earth Sciences
King Abdulaziz UniversityJeddah,
Saudi Arabia

Dr. Jyhwen Wang,
Department of Engineering Technology and Industrial Distribution
Department of Mechanical Engineering
Texas A&M University
College Station,

Prof. N. V. Sastry
Department of Chemistry
Sardar Patel University
Vallabh Vidyanagar
Gujarat, India

Dr. Edilson Ferneda
Graduate Program on Knowledge Management and IT,
Catholic University of Brasilia,
Brazil

Dr. F. H. Chang
Department of Leisure, Recreation and Tourism Management,
Tzu Hui Institute of Technology, Pingtung 926,
Taiwan (R.O.C.)

Prof. Annapurna P.Patil,
Department of Computer Science and Engineering,
M.S. Ramaiah Institute of Technology, Bangalore-54,
India.

Dr. Ricardo Martinho
Department of Informatics Engineering, School of Technology and Management, Polytechnic Institute of Leiria, Rua General Norton de Matos, Apartado 4133, 2411-901 Leiria,
Portugal.

Dr Driss Miloud
University of mascara / Algeria
Laboratory of Sciences and Technology of Water
Faculty of Sciences and the Technology
Department of Science and Technology
Algeria

International Journal of Physical Sciences

Table of Contents: Volume 10 Number 9, 16 May, 2015

ARTICLES

academicJournals

Vol. 10(9), pp. 306-310, 16 May, 2015
DOI: 10.5897/IJPS2014.4240
Article Number: 6A67ED252938
ISSN 1992 - 1950
Copyright ©2015
Author(s) retain the copyright of this article
http://www.academicjournals.org/IJPS

International Journal of Physical Sciences

Full Length Research Paper

Evaluation of tannery effluent content in Kano metropolis, Kano State Nigeria

Emmanuel BERNARD[1]* and Adepeju OGUNLEYE[2]

[1]Department of Chemistry, Nigeria Police Academy - Wudil, P. M. B. 3474, Kano, Nigeria.
[2]Department of Chemistry, Federal College of Education (Technical) – Bichi. P. M. B, 3473. Kano, Nigeria.

Received 1 December, 2014; Accepted 16 April, 2015

A field experiment was carried out to evaluate heavy metals and physiochemical concentration of tannery effluents from Kano metropolis. Fifteen samples from five selected tannery industries from Sharada and Challawa industrial estate were collected and determined for heavy metals using atomic absorption spectrophotometric method (AAS) and the result of the study showed that the range mean and standard deviation values for chromium (Cr), lead (Pb), iron (Fe) and copper (Cu) were found to be 3.33 ± 0.74 - 5.79 ± 0.96 mg/L, 0.67 ± 0.07 - 3.10 ± 1.07 mg/L, 3.53 ± 1.06 - 8.12 ± 0.69 mg/L, and 0.82 ± 0.53 - 1.51 ± 0.91 mg/L, respectively. The physiochemical values were pH 3.96 ± 1.22 - 10.60 ± 2.49, conductivity, 1554 ± 17.05 - 11410 ± 414.32 µs/cm; total suspended solid, (TSS) 1026.00 ± 170.01 - 3365.60 ± 112.63 mg/L and total dissolved solid (TDS) was 1585.00± 49.53 - 7250.00 ± 73.73 mg/L. With exception of Fe in all sites and Pb in S4, values for the other metals were above the maximum permissible limits of both the Federal Environmental Protection Agency of Nigeria (FEPA) and World Health Organization (WHO). The values for TDS for S4 and pH value for S1 to S3 were within allowable limits, but conductivity and TSS values were above the allowable limit. These findings render the effluents harmful to the environment, and there is the need to take practical steps to avoid pollution and impending health hazard.

Key words: Concentration, contamination, effluent, heavy metal, physiochemical, sewage, tannery.

INTRODUCTION

Discharges from tanneries are part of the major causes of environmental contamination in Nigeria and the world over. In recent years, large scale usage of chemicals in various human activities has grown considerably, and pollution has assumed an escalating dimension due to the continual expansion of urbanization, industrial development and agricultural activities. These pollutants find their way to aquatic ecosystem such as rivers, ponds and lakes, which pose a risk to both the human health and environment (Rehman and Anjum, 2010).

Insufficient environmental monitoring and planning often result in discharging of industrial and sewage waste into rivers and lakes which lead to gradual pollution of the water resources. Many times such wastewater is drained to the agricultural land where this polluted water is used for irrigating crops including vegetables (Aklilu et al., 2013). The consequences of untreated industrial effluent has increased water bodies pollution, loss of aquatic life

*Corresponding author. E-mail: royalhooden@yahoo.com, Tel: +2348037954633.
Author(s) agree that this article remain permanently open access under the terms of the Creative Commons Attribution License 4.0 International License

and uptake of polluted water by plants and animals, which eventually get into the human body resulting in health related problems. The situation is compounded by the fact that the common man in most of these developing countries like Nigeria does not have access to portable water, and in many instances, untreated river water is used as source of drinking water (Dan'Azumi and Bichi, 2010).

Groundwater resources are experiencing an increasing threat of pollution coming from industrial effluents which contain high concentration of metals and other physiochemical pollutants, that may be toxic, mutagenic, carcinogenic, and teratogenic, especially chromium, copper cadmium conductivity and TDS (Malarkodi et al., 2007). These effluents released on the land or into the surface water will ultimately leach to ground water and lead to contamination. Heavy metals are not easily biodegradable and lead to their accumulation in human vital organs causing varying degrees of illness on acute and chronic exposure. The accumulation also results in a series of well documented problems in plants and animals because they cannot be completely degraded (Malarkodi et al., 2007; Mustafa et al., 2010).

Chromium is a major constituent of tannery effluent tends to accumulate in living organisms, causing serious diseases and environmental pollution. It exists in oxidation states of +2, +3, and +6. The trivalent oxidation state is the most stable form of chromium and is essential to mammals in trace concentration and relatively immobile in the aquatic system due to its low water solubility. The hexavalent chromium is much more toxic to many plants, animals, and bacteria inhabiting aquatic environments (America Public Health Association (APHA), 1998; Dan'Azumi and Bichi, 2010). Hence, tannery effluents offer a wide scope of environmental problems and health hazards and are becoming more complex and critical in developing countries.

Currently, plants and microorganisms are used to remove some heavy metals such as mercury (USEPA, 2000). Plants which exhibit hyper accumulation can be used to remove heavy metals from soils by concentrating them in their bio matter. In medical usage, heavy metals are loosely defined and include all toxic metals irrespective of their atomic weight: "heavy metal poisoning" (USEPA, 2000). Consumption of water with high concentrations of TDS and conductivity have been reported to cause disorders of alimentary canal, respiratory system, nervous system, coronary system besides , causing miscarriage and cancer (Reddy and Subba, 2001).

Reduced crop contamination and improved safe food can be achieved through, reducing pollution at source, improved vegetable production and post harvest handling and using support for vegetable trading systems to improve food safety The increasing discharge of industrial wastes in this river basin is posing serious danger to the water resources and the health of people in the area.

The aim of this research work is to ascertain the level of tannery effluents pollution in the environment and advise on possible ways of reducing effluent pollution.

MATERIALS AND METHODS

Description of study area

Nigeria is located approximately between latitude 4^{o} and 14^{o} North of the equator, and between longitude 2° 2' and 15° east of the Greenwich meridian and Kano state which is ranked first in population with well over 9.0 million people, lies between latitude 12°00' and 09.4°N and longitude 08°31' and 07°29'E in Northern Nigeria. It is historically a commercial and agricultural State, and in fact the centre of commerce. The high population is brought about by the much economic and industrial activities taking place in the city. The major industries in the city include tanneries, textiles, chemicals and allied products. Kano City is located on the main watershed which separates the two main river basins in the metropolis. The main industrial areas of Kano - Bompai, Sharada, and Challawa - are located within the two river basins (Bichi and Anyata, 1999). The selected industrial sites were based on their appreciable size and location amongst other criteria.

Collection/treatment of effluent samples

Samples were collected from five tanneries sites of S1, S2 (Sharada) S3, S4 and S5 (Challawa) for three times between March and September each in plastic containers previously washed with detergents and 10% HNO_3 acid and thoroughly rinsed with de-ionized water. Suitable volume of sample was taken, and then acidified with concentrated HNO_3 to bring down the pH down to 2.0 this is to maintain the stability of the oxidation state of the various elements in solution and prevent precipitation. All the samples were taken to the laboratory and stored at 4ºC temperatures in a refrigerator till the analyses were completed. 100 cm^3 of sample was then taken and added 5 cm^3 concentrated HNO_3, and then digested. The digested samples were analyzed for chromium, iron, copper, and lead concentrations by atomic absorption spectrophotometer (Buck Scientific210 Model). Meters were used to determine the pH and conductivity while gravimetric method was used for TDS and TSS (APHA, 1998).

RESULTS AND DISCUSSION

The atomic absorption spectrophotometric analysis of heavy metal in tannery samples is summarized in Table 1.

In the present study, the range of mean for Cr, 3.33 - 5.79 mg/L has been reported in Table 1, which was higher than the maximum permissible limits of both the FEPA and WHO. In a similar study in the region 1.02 - 1.56 mg/L (Akan, 2007) and 2.49 mg/L (Dan'Azumi and Bichi, 2010), were reported. While in India 7.21 mg/L was reported (Deepali, 2010), and value as high as 9.00 mg/L has also been reported in Indian (Dikshit and Shukla, 1989). Cr is the major chemical used in tanning process and hence its discharge in the effluent was found to be higher than maximum permissible limits in all reported cases.

Table 1. Heavy metals analysis of tannery effluent samples from Kano Metropolis.

S/N	Sample	Cr (mg/L)	Pb (mg/L)	Fe (mg/L)	Cu (mg/L)
1	S1	5.79 ± 0.96	2.87 ± 1.52	5.62 ± 2.04	1.51 ± 0.91
2	S2	3.56 ± 1.60	2.67 ± 0.93	7.36 ± 3.01	1.32 ± 0.51
3	S3	4.25 ± 2.30	1.26 ± 0.32	6.00 ± 0.78	1.01 ± 0.42
4	S4	3.33 ± 0.74	0.67 ± 0.07	3.53 ± 1.06	0.82 ± 0.53
5	S5	4.16 ± 1.56	3.10 ± 1.07	8.12 ± 0.69	1.43 ± 0.33
	FEPA Max. Limit	<1.00	<1.00	20	<1.00
	WHO Max. Limit	1.00	1.00	15	0.5

Continuous discharge of Cr in low concentration has been reported to be toxic to aquatic life and has been shown to disrupt the aquatic food chain. It dominated the tannery effluent with the highest deviation from the allowable concentration and has been reported by most literatures available. Chronic exposure to chromium may be associated with allergic dermatitis in humans, permanent eye injury high blood pressure and DNA damage (Scragg, 2006)

The observed concentration range of 0.67 - 3.10 mg/L for Pb which was higher than the acceptable limit but for site S4 was reported. This findings agreed with the values reported by most researchers from both Nigeria (Sangadoyin, 1995; Dan'Azumi and Bichi, 2010) and India (Begum et al., 2009). High concentration of Pb may result in metallic poisoning that manifests in possible human carcinogenic (Bakare-Odunola, 2005). High Pb concentration may result in birth defects, mental retardation, autism, psychosis, allergies, dyslexia, hyperactivity, weight loss, shaky hands, muscular weakness, abdominal pain, head ache, irritability, joint pain, fatigue, anemia and paralysis (beginning in the forearms). It is carcinogenic and toxic, affecting, the central nervous system, the kidneys or liver, skin, bones and teeth (Hogan, 2010). In comparison with a study where a concentration of 0.1 mg/L had resulted in development of neurological problems in fetuses and children, the result obtained in this study definitely requires urgent attention by all and sundry (Fatoki et al., 2005).

The analytical results revealed 3.53 - 8.12 mg/L., as the range for Fe, which was within allowable limit. Earlier studies in the region reported 1.23 - 1.16 (Fatoki et al., 2005) and 2.14 mg/L (Rehman and Anjum, 2010; Yusuff and Sonibare, 2004) but, value as high as 4.41 - 14.556 mg/L has also been reported (Dan'Azumi and Bichi, 2010). On the contrary much lower values of 0.351 mg/L (Tariq, et al., 2006) and 0.75 mg/L (Deepali, 2010) were reported in effluent released from tanneries in India. Fe is a necessary element found in nearly all living organisms considered at the border between macro and micro elements. Iron-containing enzymes and proteins often contain heme prosthetic groups that participate in many biological oxidations and in transport (Chandra et al., 2009).

For Cu a concentration ranges of 0.82 - 1.51 mg/L was reported for Cu which was higher than the permissible value. Similarly high concentrations were earlier reported in Kano State (Dan'Azumi and Bichi, 2010) and Lagos (Sangadoyin, 1995). On the other hand Deepali (2010) reported Cu content of 0.022 mg/L in Indian. Cu is an integral part of numerous enzymes, normal copper homeostasis is essential for human growth and development, as well as for disease control in livestock and poultry, a cofactor in enzymes including ferro-oxidase (ceruloplasmin), cytochrome – c –oxidase, superoxide dismutase and others. It plays a role in iron metabolism, melanin synthesis and central nervous system function. (Fisher, 2001), but at high concentration it affects the liver and causes kidney damage and gastrointestinal distress, bone diseases, renal failure, dermatitis, pulmonary cancer, have been reported (Hogan, 2010).

From Table 2, it can be seen that the pH values for sites S4 (3.96) and S5 (10.60) were outside the allowable limit but others were within. Akan et al. (2007) in Kano and Assefa and Ayalew (2014) from Ethiopia reported values that fell within the permissible limit. pH outside permissible limit adversely affects the availability of plant nutrients, heavy metals concentrations, growth of algae and micro organism (Akan et al., 2007).

The range of conductivity obtained in this study was 1554 – 11410 µs/cm which was higher than the maximum permissible limits of both the FEPA and WHO. Other values reported were 3668- 4370 µs/cm (Assefa and Ayalew, 2014) and 6020 µs/cm (Ram, 2002). High values of conductivity indicates the presence of higher concentration of ions (Deepali et al., 2009).

TSS range of 1026.00 - 3365.60 mg/L was reported, but significantly low and high values have previously been reported 204 - 525 mg/L (Assefa and Ayalew, 2014) and 3491.9 - 9485.33 mg/L (Deepali et al., 2009).

The mean range of TDS was 1585.00 - 7250 mg/L, this value was more than the FEPA and WHO standard but for location S4 (1585.00 mg/L) with permissible value. Akan et al. (2007) report lower value of 661.4 - 1281.1 mg/L. On the contrary extremely high value of 42716.33 mg/L was reported in Indian (Raskin and Ensley, 2000;

Table 2. Physiochemical analysis of tannery effluent samples from Kano Metropolis.

S/N	Sample	pH	Cond. (µs/cm)	TSS (mg/L)	TDS (mg/L)
1	S1	7.14 ± 1.56	8360 ± 14.84	2508.40 ± 32.42	3241.00 ± 25.47
2	S2	7.09 ± 0.80	8660 ± 214.61	1026.00 ± 170.01	6010.00 ± 89.62
3	S3	7.08 ± 2.03	7920 ± 92.51	2070.00 ± 53.27	5455.00 ± 63.62
4	S4	3.96 ± 1.22	1554 ± 17.05	3365.60 ± 112.63	1585.00± 49.53
5	S5	10.60 ± 2.49	11410 ± 414.32	1575.10 ± 90.89	7250.00 ± 73.73
	FEPA max. limit	6 - 9	-	30.00	2000
	WHO max. limit	6 - 9	1000	-	2000

Deepali et al., 2009). High TDS value increases the salinity of water and thus may render it unhealthy for drinking and irrigation purposes. This makes the discharge of wastewater into surface water harmful. Consumption of water with high concentrations of TDS has been reported to cause disorders of alimentary canal, respiratory system, nervous system, coronary system besides causing miscarriage and cancer (Reddy and Subba, 2001)..Earlier analysis by Ogabiela et al. (2007) substantiated this study by reporting values for conductivity, TSS, and TDS that were higher than permissible limit in Kano.

In this study it was observed that location S4 had low pH and the concentration of heavy metals were relatively lower and it concurred with the discovery that for pH above 6 heavy metals tend to remain insoluble and more inert (Raskin and Ensley, 2000). But this finding does not clear S4 Tannery as an industry complying with standard because the acidic state of the effluent is a serious breach of acceptable practice.

Conclusions

The results of this study show that the concentration of Cr, Pb and Cu were above the limits set by FEPA and WHO. The values for pH values for some sites were within allowable limits, but others were not. Conductivity and TSS values were above the allowable limit same with most TDS values. These findings rendered the effluents harmful to the surroundings and to keep the environment healthy, discharge of untreated tannery effluent into water bodies and lands should be strongly discouraged and regular monitoring of soil, plant and water quality to ascertain the safety level should be encouraged. In addition strict legislation and stringent standard practices must be enforced to prevent the indiscriminate disposal of untreated effluent into the environment.

Conflict of Interest

The authors have not declared any conflict of interest.

REFERENCES

Akan JC, Moses EA, Ogugbuaja VO, Abah J (2007). Assessment of tannery industrial effluents from Kano metropolis, Kano State, Nigeria. J. Appl. Sci. 7:2788-2793.

Aklilu A, Mengistu S, Fisseha I (2013). Determining the Extent of Contamination of Vegetables Affected by Tannery Effluent in Ejersa Area of East Shoa, Ethiopia. Int. J. Sci. Res. Pub. 3:5.

Americal Public Health Association (APHA) (1998). Standard Methods for the examination of water and waste water, 19th edition. American Water works Association water pollution control federation publication. Washington, D.C.

Assefa W, Ayalew W (2014). Bahir Dar tannery effluent characterization and its impact on the head of Blue Nile River. Afr. J. Environ. Sci. Technol. 8(6):312–318.

Bakare-Odunola MT (2005). Determination of some metallic impurities present in soft drinks marketed in Nigeria. The Nig. J. Pharm. 4(1):51-55.

Begum A, Ramaiah M, Harikrishna I, Khan I, Veena K (2009). Heavy Metals Pollution and Chemical Profile of Cauvery River Water. E-J. Chem. 6(1): 47-52.

Bichi MH, Anyata BU (1999). Industrial Waste Pollution in the Kano River Basin. Environ. Manage. Health 10(2):112-116.

Chandra R, Bharagava RN, Yadav V, Mohan D (2009). Accumulation and distribution of toxic metals in wheat (*Triticum aestivum* L.) and Indian mustard (*Brassica campestris* L.) irrigated with distillery and tannery effluents. J. Hazard. Mater. 162:1514.

Dan'Azumi S, Bichi MH (2010). Industrial Pollution and Heavy Metals Profile of Challawa River in Kano, Nig. J. Appl. Sci. Environ. Sanitation 5(1):23-29.

Deepali KK (2010). Metals Concentration in Textile and Tannery Effluents, Associated Soils and Ground Water. New York Sci. J. 3(4):82-89.

Dikshit VP, Shukla NP (1989). Waste recycling and pollution control in Indian tanneries. Indian J. Environ. Prot. 9(3):182-86.

Fatoki OS, Lujiza N, Ogunfowokun OA (2005). Trace metal pollution in Umtata river. Water, S. A. 28(2):183.

Fisher DC (2001). Copper. In: Sullivan JB Jr. Krieger GR. Clinical Environmental Health and Toxic Exposures. 2nd Edition, Lippincott Williams & Wilkins.

Hogan CM (2010). Heavy metal. Encyclopedia of Earth. National Council for Science and the Environment. Eds Monosson E, Cleveland C. Washington DC.

Malarkodi M, Krishnasamy R, Kumaraperumal R, Chitdeshwari T (2007). Characterization of heavy metal contaminated soils of Coimbatore district in Tamil Nadu. J. Agronomy. 6(1):147-151.

Mustafa S, Ahmad T, Naum A, Shah KH, Wassum M (2010). Kinetics of chromium ion removal from tannery wastes using Amberliti IRA 400c and its hybrids. Water Air Soil Pollution 210(1-4):43-50.

Ogabiela EE, Agunwa UB, Lawal FA, Awoeye LD (2007). Analysis of tannery effluent from the confluence of discharge point at sharada industrial estate in Kano, Nigeria. J. Chem. Soc. Nig. 32(2):17–19.

Ram CS (2002). Compliance monitoring of industrial effluents standards in Nepal, State of the environment, Nepal. 6:15-16.

Raskin B, Ensley D (2000). Phytoremediation of toxic metals: Using plants to clean up the environment, John Wiley & Sons, New York, NY, USA.
Reddy PM, Subba RN (2001). Effects of industrial effluents on the ground water regime in Vishakapatnam. Pollution Res. 20(3):383-386.
Rehman A, Anjum MS (2010). Cadmium uptake by yeast, Candida tropicalis, isolated from industrial effluents and its potential use in wastewater clean–up operations. Water, Air Soil Pollution 205:149-159.
Sangadoyin AY (1995). Characteristics and control of industrial effluent generated. Pollution Environ. Manage. Health 6(4):15-18.
Scragg A (2006). Environmental Biotechnology, Oxford University Press, Oxford, UK, 2nd edition.
Tariq SR, Shah MH, Shaheen N, Khalique A, Manzoor S, Jaffar M (2006). Multivariate analysis of trace metal levels in tannery effluents in relation to soil and water- A case study from Peshawar, Pakistan. J. Environ. Manage. 79:20-29.
US Environmental Protection Agency (USEPA) (2000). EPA's Terms of Environment. U.S. Environmental Protection Agency.
Yusuff RO, Sonibare JA (2004). Characterization of textile industries' effluents in Kaduna, Nigeria and pollution implications. Global Nest: Int. J. 6(3):211-20.

academicJournals

Vol. 10(9), pp. 311-317, 16 May, 2015
DOI: 10.5897/IJPS2015.4285
Article Number: 76A62B152940
ISSN 1992 - 1950
Copyright ©2015
Author(s) retain the copyright of this article
http://www.academicjournals.org/IJPS

International Journal of Physical Sciences

Full Length Research Paper

Analytical and numerical solution of heat generation and conduction equation in relaxation mode: Laplace transforms approach

Lawal M.[1,3]*, Basant K. Jha[2], Patrick O. Akusu[3], Ahmad R. Mat Isa[1] and Nasiru R.[3]

[1]Department of Physics Faculty of Science, Universiti Teknologi Malaysia, Johor, Malaysia.
[2]Department of Mathematics, Ahmadu Bello University, Zaria, Nigeria.
[3]Department of Physics, Ahmadu Bello University, Zaria, Nigeria.

Received 16 February, 2015; Accepted 27 April, 2015

In this article analytical solution of one-dimensional heat equation in relaxation mode of heat generation and conduction using Laplace transforms method is presented. The model adopted takes into account finite velocity of heat propagation, and relaxation of heat source capacity. The properties of heat source terms in four different cases are incorporated in the model and investigated. Temperature distributions and variations with conduction mode and relaxation time are analyzed. High relaxation time is observed to lowers the temperature profile, whereas enhanced temperature distribution changes at particular values of α, and τ_g for source capacity proportional to temperature. How the steady state solution is achieved for some selected values of coefficients is also discussed.

Key words: Relaxation time, conduction mode, pulsed heat source, Laplace transforms.

INTRODUCTION

Cattaneo was the first to build an explicit mathematical theory to correct unacceptable properties of Fourier theory of heat diffusion. The arguments used were based on the kinetic theory of gases and second-order correction to propose modification of Fourier law (Cattaneo, 1948), which gives rise to the well-known hyperbolic model of heat conduction. This also leads to suitable heat conduction models that permit the finite speed of heat flow (Ozisik and Tzou, 1994; Joseph and Preziosi, 1990). In most studies of heat propagation in systems the hyperbolic model of heat conduction is used (Jose and Juan, 2011; Al-Nimr et al., 2004; Malinowski, 1993a, Saleh and Al-Nimr, 2008; Cai et al., 2006). For instance in (Malinowski, 1993b) the analytical solutions for the relaxation equation in bodies with low heat resistance, by neglecting temperature gradient were presented. It is shown that differences between parabolic and relaxation solution fluctuate as time elapses. Differences in heat generation and conduction were reported (Lewandowska, 2001) to arise due to the time characteristics of the heat source capacity. For example when the heat is of constant strength this differences slowly decrease for long times. Furthermore, solutions of both hyperbolic and parabolic heat conduction equation for temperature dependent heat source is reported to be use in analyzing normal zones in superconductors

*Corresponding author. E-mail: mohammedlawal08@yahoo.com
Author(s) agree that this article remain permanently open access under the terms of the Creative Commons Attribution License 4.0 International License

(Lewandowska and Malinowski, 2002), in which the amount of energy that is dissipated in the zone affect heat production by the heat source capacity which depends on temperature.

Although a lot of works has been done on the hyperbolic and parabolic heat conduction equation under different conditions, yet nobody as far as we know investigate the solutions for one-dimensional relaxation model of heat conduction taking into account the finite velocity of heat propagation, and relaxation of heat source capacity. Matlab program is one of the robust and most widely used program in areas of science and technology (Hübner et al., 2011). Also has many application in script design (Valipour et al., 2012), and in model development (Mohammad and Ali, 2012a; Mohammad et al., 2013). For example in irrigation engineering (Mohammad and Ali, 2012b) used the genetic coding in Matlab environment to determine the effective infiltration parameters in Furrow Irrigation. We use in this paper Matlab environment to write a script to compute the temperature profile in physical domain.

MODEL

By using the modified Fourier law Equation (1), which physically agree for a very short laser pulses and non-infinite speed of heat transport.

$$t_k \frac{\partial q}{\partial t} = -k\nabla\Theta - q, \quad (1)$$

Where t_k, k, q and Θ are the relaxation time of the heat flux, thermal conductivity, heat flux vector, and temperature respectively. Hyperbolic equation of heat conduction is obtained by substitution of Equation (1) into the energy conservation equation.

$$\rho c_p \frac{\partial \theta}{\partial t} = -\nabla . q + g, \quad (2)$$

In Equation (2) ρ is the density; c_p is specific heat at constant pressure, and g is the capacity of the internal heat source. In this paper we adopt the notion of inert heat source and transient capacity of heat source g_t as seen in Equation (3).

$$t_g \frac{\partial g_t}{\partial \tau} + g_\tau = g \quad (3)$$

For the relaxation heat conduction equation that account for both finite speed of heat propagation and the relaxation of heat source capacity Equation (4) is use.

$$t_k t_g \frac{\partial^3 \theta}{\partial t^3} + (t_k + t_g)\frac{\partial^2 \theta}{\partial t^2} + \frac{\partial \theta}{\partial t} = t_k a \frac{\partial \nabla^2 \theta}{\partial t} + \mu \nabla^2 \theta + \frac{1}{\rho c_p}(t_k \frac{\partial g}{\partial t} + g) \quad (4)$$

Where μ is thermal diffusivity, t_g is relaxation time of source capacity, the length of which depends on nature of the source. The dimensionless forms of Equations (1) to (3), are given below respectively as adopted in Lewandowska (2001), which is necessary to ensure temperature variation as a function of dimensionless displacement.

$$\frac{\partial \Phi}{\partial \tau} = -\nabla . \Phi + 2\Psi_t, \quad (5)$$

$$\frac{\partial \theta}{\partial \tau} + 2\theta = -\nabla \Phi, \quad (6)$$

$$\tau_g \frac{\partial \Psi_t}{\partial \tau} + \Psi_t = \Psi. \quad (7)$$

Transformation of Equations (5) to (7) yields the equation of heat conduction below, which permits a finite speed of heat propagation and relaxation of heat source capacity.

$$\tau_g \frac{\partial^3 \Phi}{\partial \tau^3} + (2\tau_g + 1)\frac{\partial^2 \Phi}{\partial \tau^2} + 2\frac{\partial \Phi}{\partial \tau} = \tau_g \frac{\partial}{\partial \tau}\nabla^2 \Phi + \nabla^2 + 2\frac{\partial \Psi}{\partial \tau} + 4\Psi \quad (8)$$

Where $\tau_g = \frac{\tau_g}{2\tau_k}$, and t_k is relaxation time due to delay of heat flux as a result of temperature gradient. Equation (8) is treated, considering the temperature gradient as a function of a dimensionless Cartesian co-ordinate, for $\frac{\partial^2 \Phi}{\partial Y^2} = \frac{\partial^2 \Phi}{\partial Z^2} = 0$. Thus, we obtained Equation (9).

$$\tau_g \frac{\partial^3 \Phi}{\partial \tau^3} + (2\tau_g + 1)\frac{\partial^2 \Phi}{\partial \tau^2} + 2\frac{\partial \Phi}{\partial \tau} = \tau_g \frac{\partial}{\partial \tau}\left(\frac{\partial^2 \Phi}{\partial X^2}\right) + \frac{\partial^2 \Phi}{\partial X^2} + 2\frac{\partial \Psi}{\partial \tau} + 4\Psi. \quad (9)$$

Equation (9) can be reduced to the classical hyperbolic equation of heat conduction for one dimensional case, when the relaxation time of heat capacity is set to zero.

$$\frac{\partial^2 \Phi}{\partial \tau^2} + 2\frac{\partial \Phi}{\partial \tau} = \frac{\partial^2 \Phi}{\partial X^2} + 2\frac{\partial \Psi}{\partial \tau} + 4\Psi. \quad (10)$$

We take into account the finite speed of heat propagation, relaxation of heat source capacity and heat conduction equations. We also consider temperature gradient to be a function of dimensionless displacement, and assumed high heat resistance.

MATHEMATICAL ANALYSIS

The boundary value problem of Equation (9) was solved after including four different source terms namely: (i) source with constant capacity, (ii) source capacity proportional to temperature, (iii) Dirac delta energy pulse, and (iv) source capacity proportional to time. This gives respectively,

$$\tau_g \frac{\partial^3 \Phi}{\partial \tau^3} + (2\tau_g + 1)\frac{\partial^2 \Phi}{\partial \tau^2} + 2\frac{\partial \Phi}{\partial \tau} = \tau_g \frac{\partial}{\partial \tau}\left(\frac{\partial^2 \Phi}{\partial X^2}\right) + \frac{\partial^2 \Phi}{\partial X^2} + 2\frac{\partial \Psi}{\partial \tau} + 4\Psi_c \quad (11)$$

$$\tau_g \frac{\partial^3 \Phi}{\partial \tau^3} + (2\tau_g + 1)\frac{\partial^2 \Phi}{\partial \tau^2} + 2\frac{\partial \Phi}{\partial \tau} = \tau_g \frac{\partial}{\partial \tau}\left(\frac{\partial^2 \Phi}{\partial X^2}\right) + \frac{\partial^2 \Phi}{\partial X^2} + 2\alpha\frac{\partial \Phi}{\partial \tau} + 4\alpha\Phi \quad (12)$$

$$\tau_g \frac{\partial^3 \Phi}{\partial \tau^3} + (2\tau_g + 1)\frac{\partial^2 \Phi}{\partial \tau^2} + 2\frac{\partial \Phi}{\partial \tau} = \tau_g \frac{\partial}{\partial \tau}\left(\frac{\partial^2 \Phi}{\partial X^2}\right) + \frac{\partial^2 \Phi}{\partial X^2} + 2\beta\frac{\partial(\tau)}{\partial \tau} + 4\beta\partial(\tau) \quad (13)$$

$$\tau_g \frac{\partial^3 \Phi}{\partial \tau^3} + (2\tau_g + 1)\frac{\partial^2 \Phi}{\partial \tau^2} + 2\frac{\partial \Phi}{\partial \tau} = \tau_g \frac{\partial}{\partial \tau}\left(\frac{\partial^2 \Phi}{\partial X^2}\right) + \frac{\partial^2 \Phi}{\partial X^2} + 2\beta\frac{\partial(\sin\tau)}{\partial \tau} + 4\beta\sin(\tau) \quad (14)$$

By using the Laplace transforms technique, with boundary conditions $\Phi(X,0) = \frac{\partial \Phi}{\partial \tau}(X,0) = \frac{\partial^2 \Phi}{\partial \tau^2}(X,0) = 0$, for the four different source terms respectively, solutions of Equations (11) to (14) yields:

$$\frac{d^2\bar{\Phi}}{dX^2} - \frac{A(S)}{B(S)}\bar{\Phi} + \frac{4\Psi_c}{(t_g S^2 + S)} = 0 \quad (15)$$

$$\frac{d^2\bar{\Phi}}{dX^2} - \frac{A(S)}{B(S)}\bar{\Phi} + \frac{4\alpha}{B(S)S^2} = 0 \quad (16)$$

$$\frac{d^2\bar{\Phi}}{dX^2} - \frac{A(S)}{B(S)}\bar{\Phi} + \frac{2\beta}{B(S)}(S+2) = 0 \quad (17)$$

$$\frac{d^2\bar{\Phi}}{dX^2} - \frac{A(S)}{B(S)}\bar{\Phi} + 2\beta(1+2\tau) = 0 \quad (18)$$

Where $A(S) = \tau_g S^3 + 2\tau_g S^2 + S^2 + 2S$, and $B(S) = \tau_g S + 1$ for Equations (11) to (14). However, in Equation (12), $A(S) = \tau_g S^3 + 2\tau_g S^2 + S^2 + 2S - 2\alpha S$. The α and β in Equations (16) to (18) are dimensionless coefficients that corresponding to the corresponding sources term. The solution of Equations (15) to (18) satisfying the conditions $\bar{\Phi} = 0$ for $x = 1$ and $x = 0$ is:

$$\bar{\Phi}(X,S) = K_i\left[\frac{\cosh\sqrt{\frac{A(S)}{B(S)}}}{\sinh\sqrt{\frac{A(S)}{B(S)}}} - \frac{1}{\sinh\sqrt{\frac{A(S)}{B(S)}}}\right]\sinh X\sqrt{\frac{A(S)}{B(S)}} - K_i\cosh X\sqrt{\frac{A(S)}{B(S)}} + K_i. \quad (19)$$

Where i = 1, 2, 3, and 4, $A(S)$ and $B(S)$ are as defined above with the same condition and

$$K_1 = \frac{4\Psi_c}{A(S)S} \quad (20)$$

$$K_2 = \frac{4\alpha}{A(S)S^2} \quad (21)$$

$$K_3 = \frac{2\beta(S+2)}{A(S)} \quad (22)$$

$$K_4 = \frac{2\beta}{A(S)S}\tau \quad (23)$$

The Equation (19) in Laplace transformed field is inverted for values of i = 1, 2, 3, and 4 in order to determine the temperature in physical time domain. Riemann-sum approximation (Basant and Clement, 2013) is used for the inversion of the sets of Equation (19). It involves a single summation for the numerical process. In this case the function in $\bar{\Phi}(X,S)$ is inverted to the time field.

$$\Phi(X,\tau) \cong \frac{e^{\epsilon\tau}}{\tau}\left[\frac{1}{2}\bar{\Phi}(X,\epsilon) + Re\sum_{n=i}^{N}\bar{\Phi}\left(X,\epsilon + \frac{in\pi}{\tau}\right)(-1)^n\right] \quad (24)$$

Where Re is the real part, i = $\sqrt{-1}$ is the imaginary number, N is the number of terms used in the Riemann-sum approximation. The accuracy of this method depends on the value of ϵ and the truncation error dictated by N. The ϵ is real part of Bromwich contour that is used in inverting Laplace transforms, its value must be selected so that the Bromwich contour encloses all the branch points (Tzou, 1997; Karniadakis and Beskok, 2002). For faster convergence, and reasonable results the quantity $\epsilon\tau$ should be approximately 4.7 (Vernotte, 1961). This shortens the computational time as compared to other tested values. The numerical solution is validated by considering steady state solution of Equation (25) for the first case, compared with the solution of Equation (15) for i=1 and the two results satisfy the boundary conditions x(0)= $\Phi(0)$, and x(1)= $\Phi(0)$. The pulsed energy source shows quasi-steady state behavior as the Dirac delta tends to unity. This indicates the flow is partly driven by buoyancy. This also agrees with source capacity that is proportional to time.

$$\frac{d^2\Phi}{dX^2} + 4\Psi_c = 0, \quad (25)$$

$$\frac{d^2\Phi}{dX^2} + 4\alpha\Phi = 0, \quad (26)$$

$$\frac{d^2\Phi}{dX^2} + 4\beta\delta = 0, \quad (27)$$

$$\frac{d^2\Phi}{dX^2} + 4\beta\tau = 0. \quad (28)$$

RESULT AND DISCUSSION

The results of the calculations are shown in (Figures 1 to 6). Figures 1 to 4 show the temperature profiles for the source terms that follow $\Psi = \Psi_c$, $\Psi = \alpha\Phi$, $\Psi = \beta\delta(\tau)$, and $\Psi = \beta\tau$. Using the solutions of Equations (11) to (14) for the four source terms, we write scripts that solve Equation (19) for i=1, 2, 3, and 4 by using MATLAB program in order to compute and generate the graphs. This is necessary in order to get a clear insight into the physics of the model. Different values of Ψ_c from 0.1 to 1 are used, while higher values in some cases enhance temperature profile distribution similar to the trend observed in the semi-infinite system with a time-dependent pulse energy source (Lewandowska, 2001). The resulting values of the temperature profiles $\Phi(X,\tau)$ are observed to increase for dimensionless temperature versus dimensionless time in conduction mode for the heat source capacity of constant strength. The values of τ_g are set to 1, 3, and 6

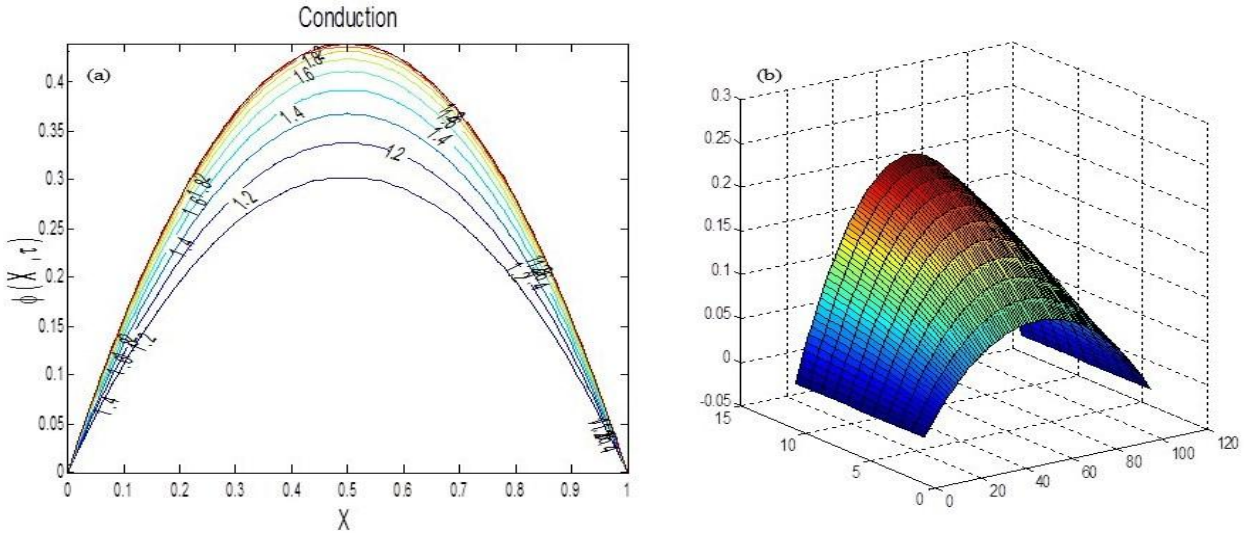

Figure 1. (a) Temperature distributions in conduction mode for constant heat source capacity, for $\tau_g = 1.$ (b) Temperature profile for $\tau_g = 3$ of the first source term.

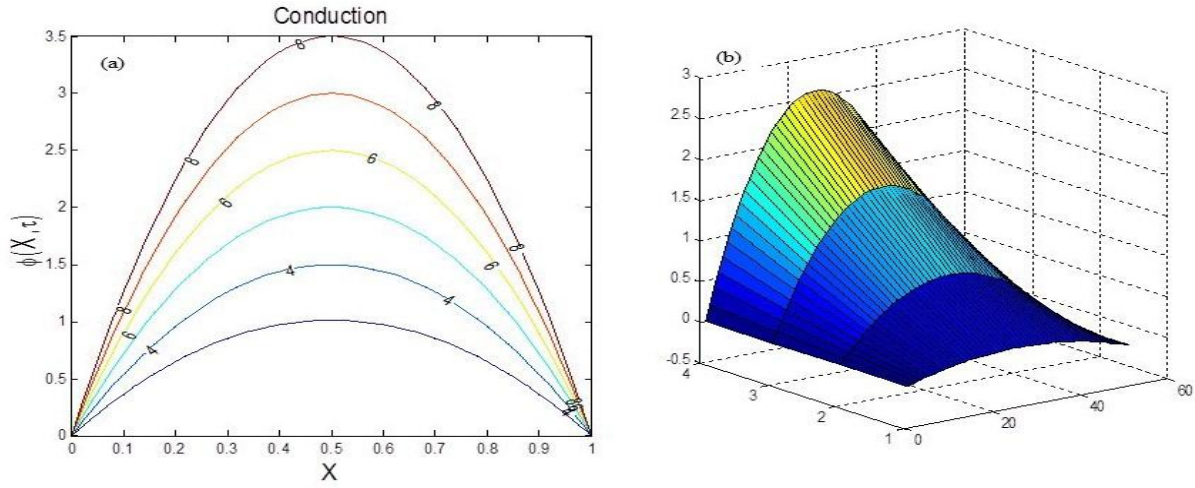

Figure 2. (a) Temperature distributions in conduction mode for source capacity proportional to temperature for for $\tau_g = 1, and\ \alpha = 1.0$, (b) Temperature profile for $\tau_g = 3$ of the second source term.

for all the four cases. In Figure 1(b), temperature profile rise as the dimensionless time slowly drop toward the direction of heat flow (Vedavarz et al., 1994), when $\tau_g = 3$ at constant source capacity. This increase of temperature in the system is caused generally by the heat generation process. Hence, dimensionless temperature distribution is indirectly proportional with the flow of heat flux as indicated in Figure 1(a). Energy is concentrated at the intermediate X for $\tau_g = 1,3,6$, in the case of conduction mode for constant heat source capacity and source capacity proportional to temperature. However, for the pulsed heat source and source capacity proportional to time shown in Figures 3(a and b) and 4(a and b), the energy is less concentrated at $\tau_g = 3.$ Figure 2(a and b) display temperature distributions when the source capacity is proportional to temperature, and for $\tau_g = 3$ respectively. Our results for this case show enhanced temperature distribution at increase value of α, and τ_g . The gradual reduction in temperature along the direction of heat flow is expected to explain the well

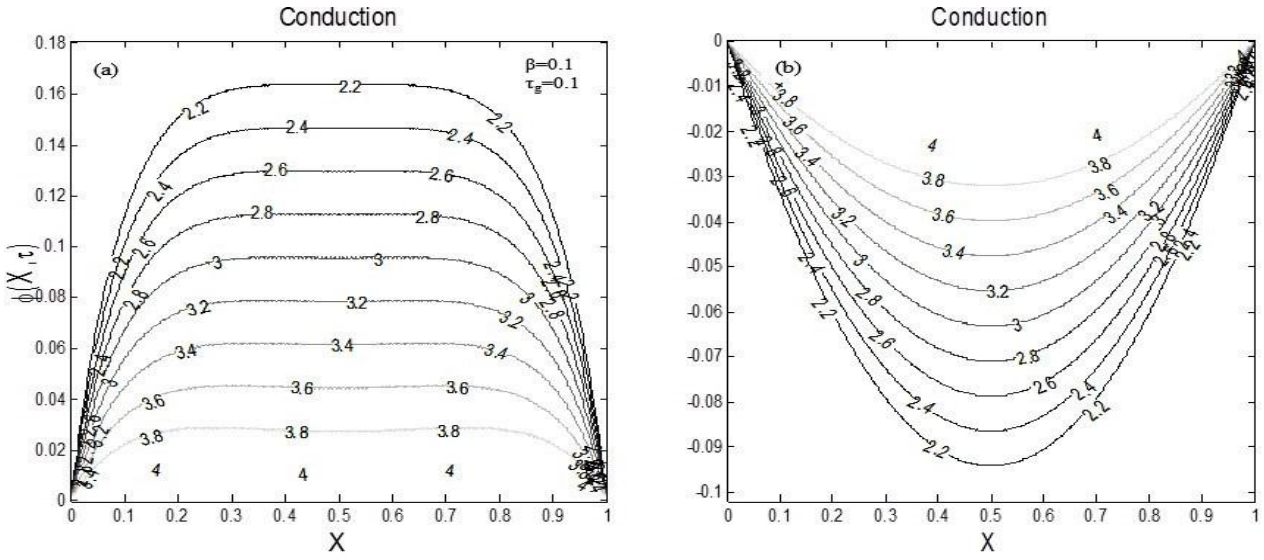

Figure 3. (a) Temperature distributions in conduction mode for pulsed heat source, (b) Temperature distributions for pulsed heat source at $\tau_g = 3$.

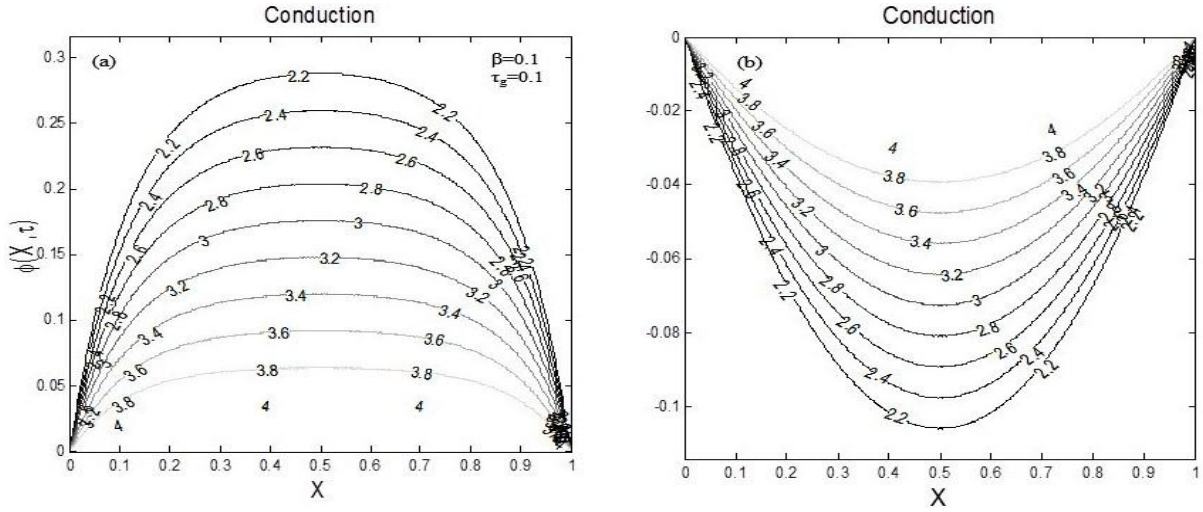

Figure 4. (a) Temperature distributions in conduction mode for source capacity proportional to time. (b) Temperature distributions for source capacity proportional to time at $\tau_g = 3$.

behavior of this model.

Figure 3(a and b) show the temperature distribution of the system, in which heat is release from a pulsed energy source. In Figure 3(a) high relaxation time lowers the temperature profile for $\tau = 0.1$, and β =1, but at higher value of τ_g the temperature profile fluctuate within the set boundary, however, the trend remains same. The temperature distribution for source capacity proportional to time in conduction mode compared to the pulsed energy source term as depicted in Figures 3(a and b) and 4(a and b). This is because when $\tau > 0$ the Dirac delta pulse approach unity, which rendered the two terms to be same at that instant that is, when $\delta(\tau) = \tau$. The little difference observed is the variation in temperature distribution, which is enhanced for source capacity proportional to time as compared to the pulsed energy source term.

Figure 5(a and b) and 6(a and b) show calculations results for the four different source terms with respect to dimensionless temperature variation versus relaxation

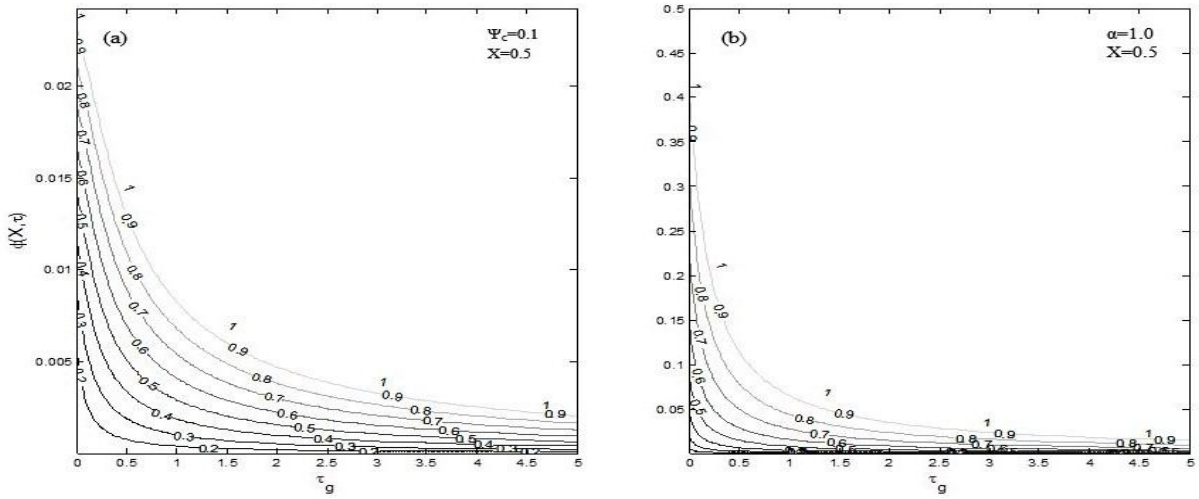

Figure 5. (a) Temperature variation with the relaxation time of source capacity calculated for the constant heat source capacity, (b) Temperature variation with the relaxation time of source capacity calculated for the source capacity proportional to temperature.

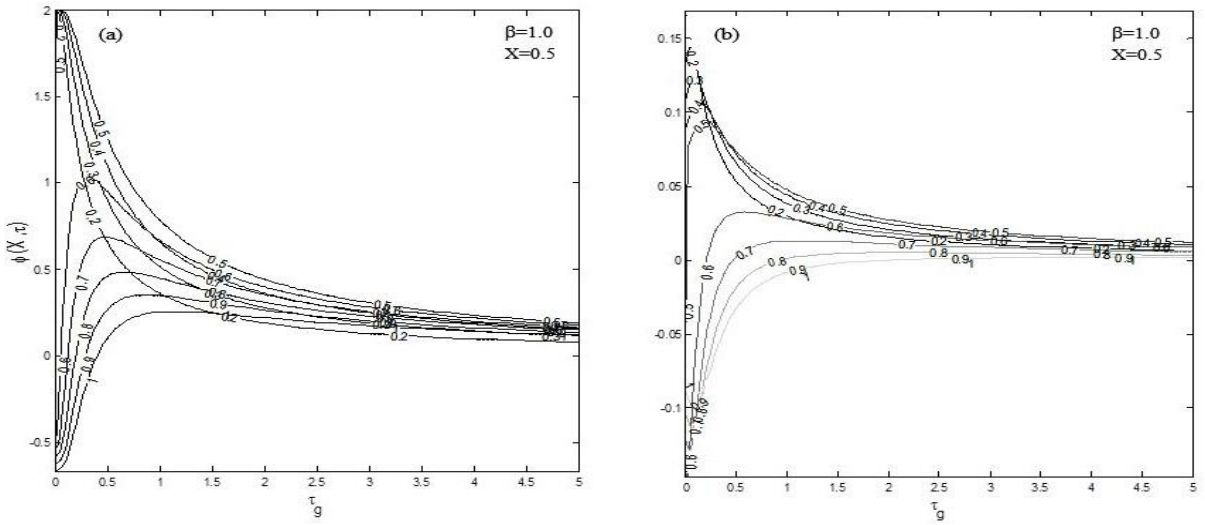

Figure 6. (a) Temperature variation with the relaxation time of source capacity calculated for the pulsed heat source, (b) Temperature variation with the relaxation time of source capacity proportional to time.

time of source capacity. In Figure 5(a and b) uniform temperature variation occurs at shorter duration, it decrease with increase of relaxation time and stabilize at high value of relaxation time, hence the mode of conduction of heat is non-diffusive for extremely short duration. In Figure 5(b) the temperature profile is observed to depend on coefficient α, which causes oscillation at higher value of α. The overall effect is enhancement of temperature profile at high values of the coefficients that is, $\Psi_c = 1, 3, 6.$ In Figure 6(a), temperature variation approaches constant value between the heat pulses of 3.5 to 5, and decrease with increase of the heat pulse from both sides of the temperature profile. The steady state solutions of Equations (26), (27) and (28) agrees with source capacity proportional to temperature, which proves the validity of the Riemann-sum approximation used in this work.

CONCLUSION

The problem of heat conduction equation for the finite

velocity of heat propagation, and relaxation of heat source capacity is solved analytically and numerically using Riemann-sum approximation. Four different expressions for dimensionless heat source capacity are considered. The effects of coefficients on temperature distribution, variation, and steady state solution are analyzed. It is observed that the temperature profile decreases when the relaxation time is high, however, at higher value of τ_g the temperature profile fluctuate within the set boundary. Furthermore, the gradual drop in temperature profile along the conduction direction agrees with the natural behavior of heat propagation.

Conflict of Interest

The authors have not declared any conflict of interest.

ACKNOWLEDGEMENT

The authors would like to thank the financial support by the Ministry of Higher Education (MOHE) Malaysia and Universiti Teknologi Malaysia (UTM) under Grant No Q.J130000.2526.06H14.

NOMENCLATURE

τ: Dimensionless time, t_k: Relaxation time of the heat flux, k: Thermal conductivity, Θ: Temperature,
Ψ: Dimensionless capacity of the internal heat source, ρ: Density, c_p: The specific heat at constant pressure, g: Capacity of the internal heat source, τ_g: Dimensionless relaxation time of source capacity, g_t: Transient heat capacity of the source, Φ: Dimensionless temperature, a: Thermal diffusivity, α: Dimensionless coefficient in expression for the Source capacity proportional to temperature, β: Dimensionless coefficient in expression for the Dirac delta pulse and Source capacity proportional to time, Ψ_c: Dimensionless coefficient in expression for the constant Source capacity, K_i: Coefficients defined by Equations (20-23),
δ: Dirac delta function, μ:Thermal diffusivity.

REFERENCES

Al-Nimr MA, Naji M, Abdallah RI (2004). Thermal behavior of a multi-layered thin slab carrying periodic signals under the effect of the dual-phase-lag heat conduction model. Int. J. Thermophysics. 25:949.
Basant KJ, Clement AP (2013). Unsteady MHD two-phase Couette flow of fluid–particle suspension. Appl. Math. Model. 37:1920.
Cai R, Chenhua G, Li H (2006). Algebraically explicit analytical solutions of unsteady 3-D nonlinear non-Fourier (hyperbolic) heat conduction. Int. J. Thermal Sci. 45:893.
Cattaneo SC (1948). Sulla conduzione de calore. Atti Semin. Mat. Fis. Univ. Modena. 3:21.
Hübner K, Sven S, Ursula K (2011). Applications and trends in systems biology in biochemistry. FEBS J. 278:2767.
Jose O, Juan JA (2011). On the stability of the exact solutions of the dual-phase lagging model of heat conduction. Nanoscale Res. Lett. 6:327.
Joseph D, Preziosi L (1990). Addendum to the paper Heat waves. Rev. Mod. Phys. 62:375.
Karniadakis G, Beskok (2002). Micro-flows Fundamentals and Simulation. Springer-Verlag, New York.
Lewandowska M (2001). Hyperbolic heat conduction in the semi-infinite body with a time-dependent laser heat source. Heat Mass Transfer. 37:333.
Lewandowska M, Malinowski L (2002). Thermal waves propagation due to localized heat inputs - the Laplace Transforms method analysis. Heat Mass Trans. 38:459.
Malinowski L (1993a). Novel model for evolution of normal zones in composite superconductors. Cryogenics. 33:728.
Malinowski L (1993b). A relaxation model for heat conduction and generation. J. Phys. D: Appl. Phys. 26:1176.
Mohammad V, Ali AM (2012a). An Evaluation of SWDC and WinSRFR Models to Optimize of Infiltration Parameters in Furrow Irrigation. Am. J. Sci. Res. P.128.
Mohammad V, Ali AM (2012b). Optimize of all effective infiltration parameters in furrow irrigation using visual basic and genetic algorithm programming. Australian J. Basic Appl. Sci. 6:132.
Mohammad V, Mohammad EB, Seyyed MRB (2013). Comparison of the ARMA, ARIMA, and the autoregressive artificial neural network models in forecasting the monthly inflow of Dez dam reservoir. J. Hydrol. 476:433.
Ozisik MN, Tzou DY (1994). On the wave theory in heat conduction. J. Heat Transfer. 116:526.
Saleh A, Al-Nimr M (2008). Variational formulation of hyperbolic heat conduction problems applying Laplace transform technique. Int. Comm. Heat Mass Trans. 35:204.
Tzou DY (1997). Macro to Microscale Heat Transfer: The Lagging Behaviour. Taylor and Francis. P. 317.
Valipour M, Banihabib ME, Behbahani SMR (2012). Monthly Inflow Forecasting using Autoregressive Artifical Network. J. Appl. Sci. 20:2139.
Vedavarz A, Kumar S, Moallemi MK (1994). Significance of non-Fourier heat waves in conduction. J. Heat Trans. 116:221.
Vernotte P (1961). Some possible complications in the phenomena of thermal conduction. Compte Rendus. 252:2191.

academicJournals

Vol. 10(9), pp. 318-323, 16 May, 2015
DOI: 10.5897/IJPS2015.4261
Article Number: 3C39B9D52942
ISSN 1992 - 1950
Copyright ©2015
Author(s) retain the copyright of this article
http://www.academicjournals.org/IJPS

International Journal of Physical Sciences

Full Length Research Paper

Study on laser etching mechanism of aluminum thin film on polyimide

Liu Xiao-Li, Xiong Yu-Qing*, Ren Ni, Yang Jian-Ping, Wang Rui, Wu Gan and Wu Sheng-Hu

Science and Technology on Vacuum Technology and Physics Laboratory, Lanzhou Institute of Physics, Lanzhou 730000, China.

Received 20 January, 2015; Accepted 16 April, 2015

In order to study the laser etching mechanism for aluminum thin film on polyimide substrate, the etching process was simulated by the finite element analysis software ANSYS, and etching profile was predicted. A theoretical model was established by comparing the simulated etching results with calculated ones; it was presumed that the etching process was firstly a thermal dominant one, then a photochemical interaction dominant one, and finally a thermal one again.

Key words: Laser etching, aluminum thin film, polyimide, etching profile.

INTRODUCTION

Based on the principle of high-power short-pulsed laser interaction with matters, laser etching was widely employed for micromachining of multi-layer thin films of metal and polymer (Liu et al., 2014; Hu et al., 2011). In this case, the absorption of laser energy occurs rapidly and only in a very thin layer of metal film on the surface, and the film is thus instantaneously evaporated and removed while the substrate is unaffected due to the precise "cool" etching process. Understanding the mechanism of laser etching is essential to predict etching result and for a better improvement of the etching quality and precision.

The mechanism of laser etching has been studied extensively, Shin et al. (2007) suggested that laser etching of multi-layer thin films of metal and polymer is a combination of photochemical evaporation and thermal melt expulsion (Srinivasan et al., 1986). Some researches investigate into the properties of laser removal of metal thin film on polymer samples was carried out theoretically and experimentally in order to understand the mechanism of laser etching (Zhang et al., 2010; Zhou et al., 2005).

In this paper, in order to predict the etching profile of laser etching for aluminum thin film on polyimide substrate and enhance the micro-processing accuracy and quality, a theoretical model, called the Srinivasan–Smrtic–Babu (SSB) model, was adopted, which takes both thermal and photochemical effects of the laser etching into consideration. Parameters for SSB model were obtained by fitting the experimental data from relevant literature (Yoon and Bang, 2005; Shin et al., 2007) and ANSYS software was employed to study the temperature distribution within aluminum thin film on polyimide (PI) substrate during 355 nm laser etching process. The operating parameters include a TEM00 Gaussian distribution laser beam, pulse repetition frequency of 20

*Corresponding author. E-mail: xiongyq@hotmail.com
Author(s) agree that this article remain permanently open access under the terms of the Creative Commons Attribution License 4.0 International License

PACS: 02.70.Dh, 52.38.Mf, 61.41 +e, 68.60.Dv, 72.15.Eb.

kHz, pulse width of 100 ns. By comparing the simulated etching results with predicted ones, the processing of 1aser energy absorption and thermal conduction were analyzed, and a mechanism of metallic film/ polyimide substrate interface separation while metallic film in solid state due to the polyimide material thermal decomposition was also proposed subsequently.

THEORETICAL MODELS

A theoretical model for PI removal by laser etching

Photochemical and thermal effects were considered for ablation of polyimide (PI), H_c is the etching depth per laser pulse by the photochemical effect according to the assumption of Beer's law (Li et al., 2006), which can be expressed as follows:

$$H_c = a_{eff}^{-1} \ln\left(\frac{F}{F_{th}}\right) \quad (1)$$

Where a_{eff}^{-1} is the absorption coefficient(cm^{-1}), F is the laser fluence per pulse (J/cm^2), and F_{th} is the threshold fluence (J/cm^2).

When processing PI, the thermal effect is non-ignorable, the single pulse etching depth expressed by H_T, from pseudo-zeroth order rate law:

$$-\frac{dc}{dt} = kc \Rightarrow -\int_{c_0}^{c}\frac{dc}{c} = k\int_0^t dt \quad (2)$$

$$H_T = k_0 \cdot e^{-E/RT} \quad (3)$$

Where k_0 is the effective frequency factor (μm/pulse), E is the activation energy (kJ/cm^3), R is the gas constant (371 $J/(cm^3 \cdot K)$), and T is the temperature averaged in some manner over the irradiated region and is controlled by the incident fluence and the photon absorption dynamics of the PI. Temperature within the laser exposed region is both time and position dependent. In the absence of knowledge of the exact functional dependence, it is only possible to proceed phenomenologically by assuming a one dimensional heat flow. The fluence dependence of local temperature can be modeled by an expression similar to that proposed by Yung et al. (2000):

$$T(x) = \frac{a_{eff} \cdot F}{\rho \cdot C_p} \cdot e^{a_{eff} \cdot x} \quad (4)$$

Where ρ is density(kg/cm^3), C_P is heat capacity(J/kg·K), and x is the etching depth(cm).

Calculate the T_{avg} (average temperature) from x=0 to x=d_p:

$$T_{avg} = \frac{\int_0^{dp} T(x)\,dx}{\int_0^{dp} dx} = \frac{a_{eff} \cdot F}{\rho \cdot C_p} \int_0^{dp} e^{-x a_{eff}}\,dx = \frac{a_{eff} \cdot F}{\rho \cdot C_p} \cdot \frac{1}{dp}\left(1 - e^{-a_{eff} dp}\right) \quad (5)$$

It can be simplified as:

$$dp = \frac{1}{a_{eff}} \cdot \ln\frac{F}{F_{th}} \Rightarrow dp \cdot a_{eff} = \ln\frac{F}{F_{th}} \quad (6)$$

By combining Equation (5) and (6), it can be obtained that:

$$T_{avg} = \frac{a_{eff}}{\rho \cdot C_p \cdot F}(F - F_{th}) \quad (7)$$

By putting Equation (7) into Equation (3), H_T (The etching depth by the photothermal effect) can be obtained as:

$$H_T = k_0 \cdot e^{[(-E \cdot \ln F/F_{th})/(a_{eff}(F - F_{th}))]} \quad (8)$$

Table 1. Parameters of PI for 355 nm UV laser etching.

Parameter	Values
F_{th}(J/cm^2)	0.1
a_{eff}(cm^{-1})	0.2×10^5
k_0(μm/pulse)	8.86
E^*(kJ/cm^3)	207.6×10^3

Where $E^* = \frac{E \cdot \rho \cdot C_p}{a_{eff}}$ is the effective activation energy (kJ/cm^3), when photochemical and thermal effects were take into consideration, the etching depth per laser pulse, H_{PI} can be expressed as follows:

$$H_{PI} = \frac{1}{a_{eff}} \cdot \ln\frac{F}{F_{th}} + k_0 \cdot e^{[(-E \cdot \ln F/F_{th})/(a_{eff}(F - F_{th}))]} \quad (9)$$

By putting parameters in Table 1 into Equation (9), theoretical relationship between etching depth and fluence can be obtained, as shown in Figure 1.

In Figure 1, which shows the theoretical results in logarithmic scale, the etching depth will maintain at a constant value as the laser fluence increases. When the laser fluence is smaller than 1 J/cm^2, while photochemical effect is dominant, the etching depth as a logarithmic function increases rapidly, and then stays at a constant value. Reversely, the etching depth by thermal effect increases dramatically in the region of laser fluence greater than 5 J/cm^2. Although the etching depth is an exponential function of laser fluence, the logarithmic function in the exponent reduces the etching rate rapidly in the region of fluence greater than 25 J/cm^2. This indicates that a laser fluence greater than a certain value contributes little to the etching depth. Thus, it is meaningless to increase the laser fluence above this value.

A theoretical model for Al removal by laser etching

Considering that thermal effect is dominant during laser etching process of Al, we adopt a theoretical model which takes only thermal effects into account, to predict the etching depth of laser etching of Al films. H_{AL} can be expressed as follows:

$$H_{AL} = H_T = k_0 \cdot e^{[(-E \cdot \ln F/F_{th})/(a_{eff}(F - F_{th}))]} \quad (10)$$

By putting parameters of Al in Table 2 into Equation (10), theoretical relationship between etching depth and laser fluence can be obtained, as shown in Figure 2. Figure 2 shows the theoretical results of etching depth considering only thermal effect in decimal scale. In the region of fluence smaller than 3.2 J/cm^2, the etching depth is not measurable; and in the region of fluence greater than 4 J/cm^2, the etching depth increases rapidly.

SIMULATION SOLUTION

Here, the adopted equations for laser-material interaction will be presented. Non-steady-state temperature distribution within thin film and substrate can be obtained by applying heat transfer and phase change model of laser heating. Ignoring gas and liquid dynamic effects (Li et al., 2008), differential equation describing temperature $T(x,y,t)$ of this process is:

$$c(T)\rho\frac{\partial T(x,y,t)}{\partial t} = \nabla\left(K(T) \cdot \nabla T(x,y,t) + Q(x,y,T,t)\right) \quad (11)$$

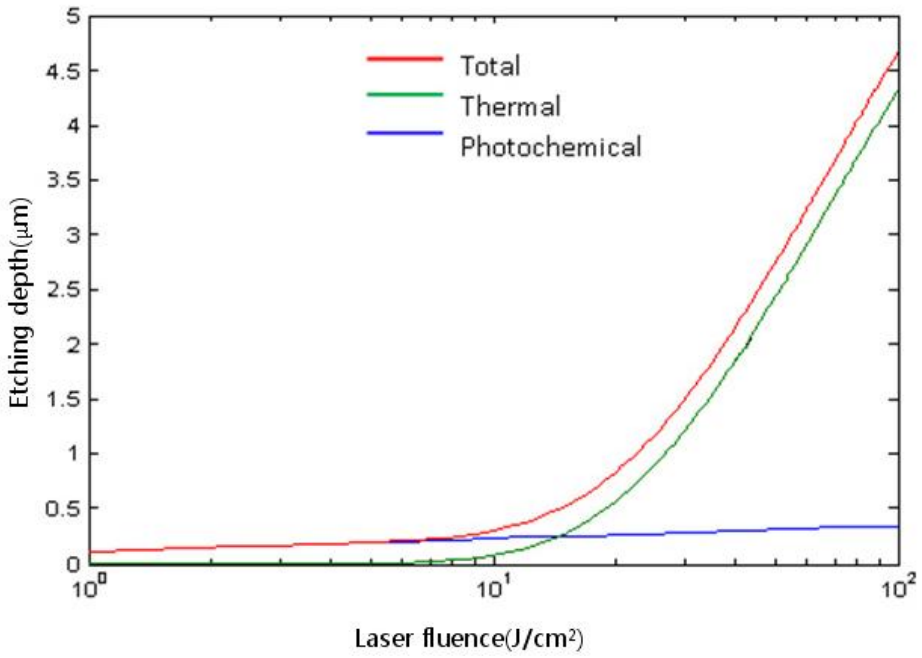

Figure 1. Relationship between etching depth and laser fluence for PI etched by 355 nm UV laser.

Table 2. Parameters of Al for 355 nm UV laser etching.

Parameter	Values
F_{th}(J/cm^2)	0.32
a_{eff}(cm^{-1})	5.917×10^5
k_0(μm/pulse)	78
E^*(kJ/cm^3)	1.13×10^7

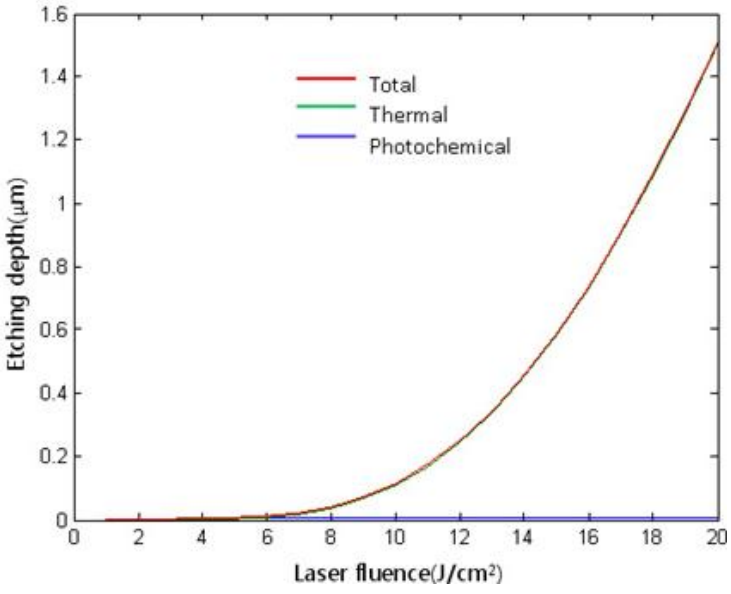

Figure 2. Relationship between etching depth and laser fluence for Al etched by 355 nm UV laser.

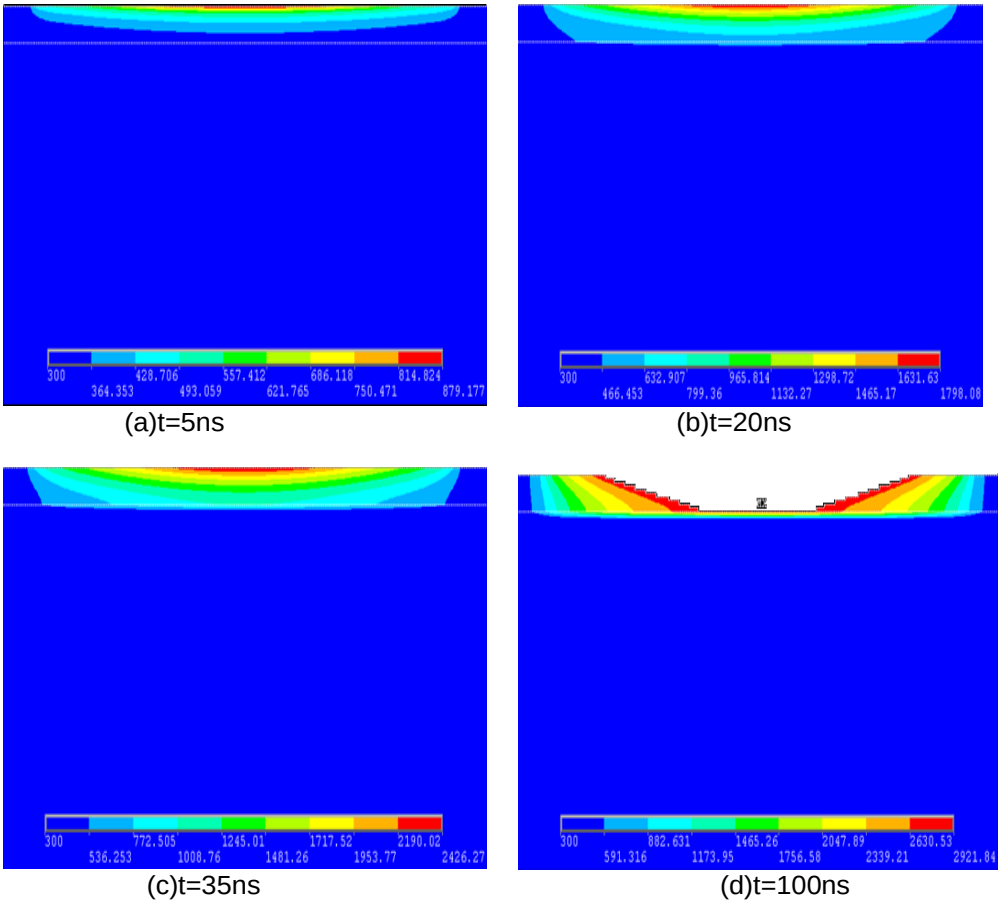

(a)t=5ns (b)t=20ns

(c)t=35ns (d)t=100ns

Figure 3. Simulated temperature field caused by laser irradiation with different times (Different color represents different temperature).

Where c is specific heat capacity, ρ is material density, K is thermal conductivity, and Q is the heat generation rate. The initial temperature before laser irradiation equals to environmental temperature:

$$T(x,y,0) = T_{env} \quad (12)$$

The boundary conditions for temperature of the heated top surface and the other surfaces are different. Because of the high heat flow gradients during laser heating, no heat is lost from the heated side. Therefore, the Neumann boundary condition was used for boundary at y=0 (Hu and Yin, 1997). However, as the laser affected depth is much smaller than thickness of thin film, the opposite surface is assumed to stay at environmental temperature according to the Dirichlet boundary condition, expressed as follows:

$$\frac{\partial T(x,y,t)}{\partial z}\Big|_{z=0} = 0 \quad (13)$$

$$T(x,y,t)|_{z=thickness\ of\ sample} = T_{env} \quad (14)$$

According to the theory of heat transfer in solid, analytical solution to Equation (11) can be obtained when laser power density is independent upon time. However, as one laser pulse generally offers several times the amount of energy required for one unit mass to rise from room temperature to evaporation temperature of Al within a very short period of time, the large heat flow gradient makes thermal properties of Al thin film temperature-dependent. Therefore, finite element method implemented in ANSYS was used to obtain the approximate numerical solution of the nonlinear model. This paper is based on theoretical and simulative analysis. The process of laser removal of Al thin film on PI samples was studied and the mechanism of the laser etching was analyzed.

Numerical simulation for process of etching of aluminum thin film on PI

Before simulation, the constant temperature boundary was assumed (T_{int}=300 K). Figure 3 shows the temperature distribution during the laser etching of Al/PI with different irradiation pulse. Figure 3(a) displays

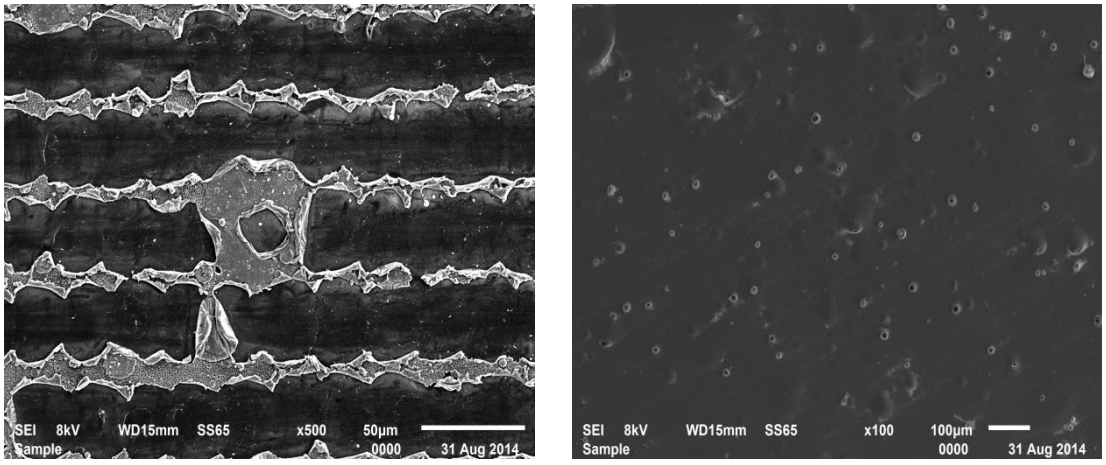

(a) (b)

Figure 4. SEM images of etched morphology with different irradiation pulse.

temperature distribution within Al/PI with a laser output power of 4W and an irradiation pulse of 5 ns. It can be seen that the maximum center temperature on the surface is 814.824 K and the interface temperature retains 300 K, which means that the heat does not transfer to the substrate, and laser etching is a thermal process, for which the excitation energy is instantaneously transformed into heat. Over a period of time, as shown in Figure 3(b), temperature at interface reaches 466.453 K, which is lower than the substrate's decomposing temperature, 500 K. Figure 3(c) shows temperature distribution within Al/PI for a pulse of 35 ns, it can be seen that the maximum temperature at the interface reaches about 772.505 K, which is higher than substrate's decomposing temperature, which can result in substrate decomposition, and the pressure formed cause a state of separation between Al films and PI substrate. Meanwhile, heat conduction was blocked and the total energy is transformed to heat, induce rapid evaporation of Al films. As shown in Figure 3(d), it can be found that with the laser irradiation pulse change from 5 ns to 100 ns, the surface temperature increases gradually and Al thin film was removed rapidly.

Experimental etching of Al thin film on PI was conducted to verify the simulated results. It shown that the etched Al thin film presents different edges with different irradiation pulse, corresponded to different laser fluence. The coarse edge of etched thin film in Figure 4(a) indicate that it was peeled off by pressure formed by decomposition of PI, and Figure 4(b) shows the bubbles formed on surface of PI caused by decomposition clearly.

CONCLUSION

By comparing of the simulated and calculated etching results, it can be concluded that the etching process was firstly a thermal interaction dominant one, aluminum thin film absorbs portion of the laser energy and transferred it into heat; then, when the temperature raised to decomposing temperature of polyimide, a photochemical interaction was dominant and polyimide at interface decomposed, a pressure is formed above the interface and peeled aluminum thin film off from polyimide substrate; Finally, temperature of floated aluminum increased and gasified, thermal mechanism is determinant again at this stage. The simulation was verified by experiment, and the simulated results can be used to optimize the etching parameters to obtain a smooth etching edge.

Conflict of Interest

The authors have not declared any conflict of interest.

ACKNOWLEDGEMENT

This work is supported by National Natural Science Foundation of China (NSFC. 51135005)

REFERENCES

Liu TH, Hao ZQ, Gao X, Liu ZH, Lin JQ (2014). Shadowgraph investigation of plasma shock wave evolution from Al target under 355-nm laser ablation. Chinese Phys. B 23(8):085203.

Hu HF, Ji Y, Hu Y, Ding XY, Liu XW, Guo JH, Wang XL, Zhai HC (2011). Thermal analysis of intense femtosecond laser ablation of aluminum. Chinese Phys. B. 20(4):044204.

Srinivasan V, Smrtic MA, Babu SV (1986). Excimer laser etching of polymers. J. App. Phys. 59(11):3861-3867.

Zhang F, Duan J, Zeng XY, Li XY (2010). 355 nm DPSS UV

Laser Micro-Processing For Semiconductor and Electronics Industry, Proc. SPIE. 7584:75840-75850.
Zhou XL, Wen W, Zhang JS, Sun DB (2005). A mathematical model of the removal of gold thin film on polymer surface by laser ablation. Surf. Coat. Tech. 190:260–263.
Yoon KK, Bang SY (2005). Modeling of polymer ablation with excimer lasers. J. Korean Soc. Precision Eng. 22(9):60-68.
Shin BS, Oh JY, Sohn H (2007). Theoretical and experimental investigations into laser ablation of polyimide and copper films with 355-nm Nd: YVO_4 laser. J. Mater. Process. Tech. 187-188:260-263.
Li L, Zhang D, Li Z, Guan L, Tan X, Fang R, Hu D, Liu G (2006). The investigation of optical characteristics of metal target in high power laser ablation. Physica B. 383(2):262-266.
Yung WKC, Liu JS, Man HC, Yue TM (2000). 355 nm Nd:YAG laser ablation of polyimide and its thermal effect. J. Mater. Process. Technol. 101:306~311.
Li J, Peterson GP, Cheng P (2008). Dynamic characteristics of transient boiling on a square platinum microheater under millisecond pulsed heating. Int. J. Heat Mass Tran. 51:273–282.
Hu B, Yin HM (1997). On Critical Exponents for the Heat Equation with a Mixed Nonlinear Dirichlet-Neumann Boundary Condition. J. Math. Anal. Appl. 209:683-711.

academicJournals

Vol. 10(9), pp. 324-328, 16 May, 2015
DOI: 10.5897/IJPS2015.4303
Article Number: 27DD7F353011
ISSN 1992 - 1950
Copyright ©2015
Author(s) retain the copyright of this article
http://www.academicjournals.org/IJPS

International Journal of Physical Sciences

Full Length Research Paper

Solutions of the Klein-Gordon equation for l≠0 with position-dependent mass for modified Eckart potential plus Hulthen potential

M. R. Shojaei and M. Mousavi*

Department of Physics, University of Shahrood, P. O. Box 36155-316, Shahrood, Iran.

Received 30 March, 2015; Accepted 27 April, 2015

In this paper we solve analytical the position-dependent effective mass Klein–Gordon equation for modified Eckart potential plus Hulthen potential with unequal scalar and vector potential for l≠0. The Nikiforov-Uvarov (NU) method is used to obtain the energy eigenvalues and wave functions. We also discuss the energy eigenvalues and wave functions for the constant-mass case. The wave functions of the system are taken in the form of the Laguerre polynomials. The results are the exact analytical. The energy eigenvalues and wave functions are interesting for experimental physicists.

Key words: Klein–Gordon equation, modified Eckart potential plus Hulthen potential, Nikiforov-Uvarov (NU) method, position-dependent mass.

INTRODUCTION

The description of phenomena at higher energy requires the investigation of a relativistic wave equation. Therefore one of the interesting problems in nuclear and high energy physics is to obtain analytical solution of the Klein - Gordon, Duffin – Kemmer - Petiau and Dirac equations for mixed vector and scalar potentials (Oyewumi and Akoshile, 2010). The exact solutions of the wave equations (non-relativistic or relativistic) are very important since they contain all the necessary information regarding the quantum system under consideration. However, analytical solutions are possible only in a few simple cases such as the hydrogen atom and the harmonic oscillator (Schiff, 1955; Landau and Lifshitz, 1977).

If we consider the case where the interaction potential is not strong enough to create particle-antiparticle pairs, we can apply the Klein-Gordon equation to the treatment of a zero-spin particle and apply the Dirac equation to that of a 1/2-spin particle (Cheng and Dai, 2007). Spin and pseudospin symmetries are SU(2) symmetries of a Dirac Hamiltonian with vector and scalar potentials. They are realized when the difference, $\Delta(r)=V(r)-S(r)$, or the sum, $\Sigma(r)=V(r)+S(r)$, are constants. The near realization of these symmetries may explain degeneracies in some heavy meson spectra (spin symmetry) or in single-particle energy levels in nuclei (pseudospin symmetry), when these physical systems are described by relativistic mean-field theories (RMF) with scalar and vector potentials (Ginocchio, 2005; Feizi et al., 2013; Alberto et al., 2013).

The kind of various methods have been used for the exact solutions of the Klein – Gordon equation and Dirac

*Corresponding author. E-mail: nuclear.physics2020@gmail.com
Author(s) agree that this article remain permanently open access under the terms of the Creative Commons Attribution License 4.0 International License

equation such as the Supersymmetry Quantum Mechanics (Jia et al., 2006; Astorga et al., 2012; Feizi et al., 2011). Asymptotic iteration method (AIM) (Ciftci et al., 2003; O¨zer and Le´vai, 2012) and Nikiforov-Uvarov (NU) (Shojaei et al., 2014; Berkdemir et al., 2006; Rajabi and Hamzavi, 2013) and others.

The Klein – Gordon and Dirac wave equations are frequently used to describe the particle dynamics in relativistic quantum mechanics with some typical potential by using different methods (Ikot et al., 2011). For example, Kratzer potential (Qiang, 2004, 2003), Woods-Saxon potential (Berkdemir et al., 2006; Guo and Sheng, 2005). Scarf potential (Xue-Cai et al., 2005; Zhang et al., 2005). 16 Hartmann potential (Chen, 2005; de Souza Dutra and Hott, 2006), Rosen Morse potential, (Yi et al., 2004; Alhaidari, 2001) and Hulthen potential (Farrokh et al., 2013).

The problem of the non-relativistic and relativistic wave equations with spatially dependent masses has been attracting much intention in the literature. Systems with position-dependent mass have been found to be very useful in studying the physical properties of various microstructures, such as semiconductor heterostructure (VonRoos, 1983). Quantum liquids (Arias de Saavedra et al., 1994), quantum wells and quantum dots (Serra and Lipparini, 1997), 3He clusters (Barranco et al., 1997), compositionally graded crystals (Geller and Kohn, 1993; Jia et al., 2012) etc.

A lot of studies have been performed to obtain the solutions of the Schrodinger, Klein-Gordon and Dirac equations with position-dependent mass for different potentials (Arda et al., 2010, 2009). For example, Aygun et al. (2012), Jia et al. (2012), Antia et al. (2012) and Souza Dutra considered position-dependent effective mass (Jia and de Souza Dutra, 2006).

In this paper, we attempt to solve approximately Klein – Gordon equation for l≠0 with modified Eckart potential plus Hulthen potential for the scalar and vector potential with a spatially dependent mass by using the Nikiforov – Uvarov (NU) method. We also discuss the limit of the scalar and vector potential with constant mass (Shojaei et al., 2014; Cheng and Dai, 2007).

REVIEW of NIKIFOROV -UVAROV (NU) METHOD

The NU method is based on the solution of a generalized second order linear differential equation with special orthogonal functions. The NU method has been used to solve the Schrodinger, Dirac, and Klein-Gordon wave equations for a certain kind of potential. In this method the differential equations can be written as follows (Shojaei et al., 2014; Cheng and Dai, 2007):

$$\Psi''(s)+\frac{\tilde{\tau}(s)}{\sigma(s)}\Psi'(s)+\frac{\tilde{\sigma}(s)}{\sigma^2(s)}\Psi(s)=0 \quad (1)$$

Where σ(s) and $\tilde{\sigma}(s)$ are words of second degree and $\tilde{\tau}(s)$ is a first degree polynomials. In obtaining the exact solution to Equation (1) we set the wave function as:

$$\Psi(s)=\phi(s)y(s) \quad (2)$$

And on substituting Equation (2) into Equation (1) reduces Equation (1) into hyper geometric type,

$$\sigma(s)y''(s)+\tau(s)y'(s)+\lambda y(s)=0 \quad (3)$$

Where Φ(s) is defined as a logarithmic derivative

$$\frac{\phi'(s)}{\phi(s)}=\frac{\pi(s)}{\sigma(s)} \quad (4)$$

Where π(s) is most a first degree polynomial.

The other part, y(s), is the hyper geometric-type function whose polynomial solutions are given by the Rodrigues relation.

$$y_n(s)=\frac{B_n}{\rho_n}\frac{d^n}{ds^n}(\sigma^n(s)\rho(s)) \quad (5)$$

Where B_n is the normalizing constant and the weight function ρ(s) must satisfy the following condition:

$$\frac{d\omega(s)}{ds}=\frac{\tau(s)}{\sigma(s)}\omega(s) \quad (6)$$

Where $\omega(s)=\sigma(s)\rho(s)$.

$$\tau(s)=\tilde{\tau}(s)+2\pi(s) \quad (7)$$

It is necessary that the classical orthogonal polynomials τ (s) be equal to zero to some point of an interval (a, b) and its derivative at this interval at σ(s) > 0 will be negative, that is

$$\frac{d\tau(s)}{ds}\prec 0 \quad (8)$$

Therefore, the function π(*s*) and the parameter λ required for the NU-method are defined as follows:

$$\pi(s)=\frac{\sigma'(s)-\tilde{\tau}(s)}{2}\pm\sqrt{\left(\frac{\sigma'(s)-\tilde{\tau}(s)}{2}\right)^2-\tilde{\sigma}(s)+k\sigma(s)}\,,$$
$$\lambda=k+\pi'(s) \quad (9)$$

The k-values in the square-root of Equation (9) are possible to evaluate if the expression under the square root must be square of polynomials. This is possible if its discriminant is zero. Thus, a new eigenvalue equation

for the second-order differential equation becomes:

$$\lambda = \lambda_n = -n\tau'(s) - \frac{n(n-1)}{2}\sigma''(s), \quad (n = 0,1,2,...) \qquad (10)$$

Where τ (s) is as defined in Equation (7) and on comparing Equations (9) and (10), we obtain the energy eigenvalues.

SOLUTIONS OF THE KLEIN-GORDON EQUATION For l≠0

The three-dimensional radial arbitrary l-state K-G equation with position-dependent mass is written as follows (Greiner, 2000):

$$\frac{d^2U(r)}{dr^2} + \frac{1}{\hbar^2c^2}\left\{\left[E - V(r)\right]^2 - \left[Mc^2 + S(r)\right]^2 - \frac{\ell(\ell+1)}{r^2}\hbar^2c^2\right\}U(r) = 0 \qquad (11)$$

Where M is the rest mass, E is the relativistic energy, c is the speed of light ,ħ is the reduced Planck's constant, *V* (*r*) and *S*(*r*) are vector and scalar potentials, respectively. From Equation (11), we have

$$\frac{d^2U(r)}{dr^2} + \frac{1}{\hbar^2c^2}\left\{E^2 - M^2c^4 - 2EV(r) - 2Mc^2S(r) + V^2(r) - S^2(r) - \frac{\ell(\ell+1)}{r^2}\hbar^2c^2\right\}U(r) = 0 \qquad (12)$$

Vector and scalar the potential by investigation modified Eckart potential plus Hulthen potential are respectively written as:

$$V(r) = \coth(\alpha r) + \frac{v_0}{(1-e^{-2\alpha r})}, \quad S(r) = \coth(\alpha r) + \frac{s_0}{(1-e^{-2\alpha r})} \qquad (13)$$

Where s_0, v_0, the potential depth, and *α* are constant. We emblazon the position-dependent mass in the specific form:

$$M(r) = m_0 + m_1\coth(\alpha r) + m_2\frac{1}{(1-e^{-2\alpha r})} \qquad (14)$$

If we define a new variable $U(r) = rR(r)$ and substituting it in to Equation (12), we obtain the radial equation of Klein – Gordon equation as

$$\frac{d^2R(r)}{dr^2} + \frac{2}{r}\frac{dR(r)}{dr} + \frac{1}{\hbar^2c^2}\left\{E^2 - M^2c^4 - 2EV(r) - 2Mc^2S(r) + V^2(r) - S^2(r) - \frac{\ell(\ell+1)}{r^2}\hbar^2c^2\right\}R(r) = 0 \qquad (15)$$

We can evaluate the new improved approximation scheme by using the following pekeris-type approximation that is valid for *α* ≤ 1, (Hill, 1954).

$$\frac{1}{r^2} \approx \frac{4\alpha^2}{(e^{-2\alpha r} - 1)^2} \qquad (16)$$

Using the transformation $s = (1 - \exp(-2\alpha r))$ Equation (15) brings into the form

$$\frac{d^2R(r)}{dr^2} + \frac{(-4\alpha)}{s}\frac{dR(r)}{dr} + \frac{1}{\hbar^2c^2}\left\{E^2 + \frac{(2-s)^2}{s^2} + \frac{v_0^2}{s^2} + \frac{2(2-s)v_0}{s^2} - \frac{2E(2-s)}{s} - \frac{2Ev_0}{s} - m_0^2c^4 - \frac{\left[m_1c^2(2-s) + m_2c^2\right]^2}{s^2} - \frac{2m_0c^2\left[m_1c^2(2-s) + m_2c^2\right]}{s} - \frac{(2-s)^2}{s^2} - \frac{s_0^2}{s^2} - \frac{2(2-s)s_0}{s^2} - \frac{2m_0c^2(2-s)}{s} - \frac{2m_1c^2(2-s)^2}{s^2} - \frac{2m_2c^2(2-s)}{s^2} - \frac{2m_0c^2s_0}{s} - \frac{2m_1c^2s_0(2-s)}{s^2} - \frac{2m_2c^2s_0}{s^2} - \frac{4\alpha^2\ell(\ell+1)}{s^2}\hbar^2c^2\right\}R(r) = 0 \qquad (17)$$

We can write the Equation (17) as summarized:

$$R'' + \frac{(-4\alpha)}{s}R' + \frac{1}{s^2}\left[A's^2 + B's + c'\right]R = 0 \qquad (18)$$

Where the parameters A', B' and C' are defined as follows:

$$A' = \frac{1}{\hbar^2c^2}\left\{\left(E^2 + 2E\right) - \gamma\right\}$$

$$B' = \frac{1}{\hbar^2c^2}(aE + b) \qquad (19a)$$

$$C' = \frac{1}{\hbar^2c^2}\left\{\left(v_0 + 2\right)^2 - \left(s_0 + 2\right)^2 - \left(2m_1c^2 + m_2c^2\right)\left(2m_1c^2 + m_2c^2 + 2s_0 + 4\right)\right\} - 4\alpha^2\ell(\ell+1)$$

And,

$$\gamma = \left(m_0c^2 - m_1c^2\right)\left(m_0c^2 - m_1c^2 - 2\right)$$

$$a = -\left(4 + 2v_0\right) \qquad (19b)$$

$$b = 2m_1c^2\left(m_1c^2 + m_2c^2 - 2m_0c^2 + s_0 + 4\right) - 2m_0c^2\left(m_2c^2 + s_0 + 2\right) + 2\left(s_0 - v_0 + m_2c^2\right)$$

Now we use the NU method to solve the Equation (18). Comparing Equation (1) and (18) we get

$$\tilde{\tau} = -4\alpha, \quad \sigma(s) = s, \quad \tilde{\sigma}(s) = A's^2 + B's + C' \qquad (20)$$

Substituting the expressions above into Equation (9), we have the function *π*(*s*) as

$$\pi(s) = 1 \pm \left[\left(-A'\right)^{1/2}s \pm (1 - C')\right] \text{ for } k = B \pm 2\sqrt{A'(C'-1)} \qquad (21)$$

With respect to Condition of Equation (8), the best choice for k and *π* as follows:

$$\pi(s) = 1 - \left[\left(-A'\right)^{1/2} s - (1 - C') \right] \text{ for } k = B - 2\sqrt{A'(C'-1)} \quad (22)$$

By following the equation $\lambda = \lambda_n$ in the NU method, we have the energy eigenvalues equation

$$B'^2 = [(2n+1) + 2(1-C')^{1/2}]^2 (-A') \quad (23)$$

And use Equation (19a) and Equation (23)

$$a^2E^2 + b^2 + 2abE = -\alpha'\hbar^2c^2(E^2 + 2E - \gamma),$$
$$\alpha' = [(2n+1) + 2(1-C')^{1/2}]^2 \quad (24)$$

By solving the Equation (24) the exact energy eigenvalues of the K-G equation for this system are derived as:

$$E_{n,\ell} = \frac{-(ab + \alpha'\hbar^2c^2) \pm \sqrt{\alpha'\hbar^2c^2[(1+\gamma)(\alpha'\hbar^2c^2 + a^2) - (a-b)]}}{2(\alpha'\hbar^2c^2 + a^2)} \quad (25)$$

Let us now find the corresponding eigenfunctions for this system. Firstly, we find the first part of the eigenfunctions by Using Equation (4)

$$\phi(s) = s^{[1+(1-c')^{1/2}]} \exp[-(-A')^{1/2} s] \quad (26)$$

Secondly, we calculate the weight function as

$$\rho(s) = s^{2[2\alpha + \frac{1}{2} + (1-c')^{1/2}]} \exp[-2(-A')^{1/2} s] \quad (27)$$

Which the second part of the wave function gives by Equation (5) as

$$y_n = B_n s^{-2[2\alpha + \frac{1}{2} + (1-c')^{1/2}]} \exp[2(-A')^{1/2} s] \frac{d^n}{ds^n} [s^{n+2[2\alpha + \frac{1}{2} + (1-c')^{1/2}]} \exp[-2(-A')^{1/2} s]] \quad (28)$$

By using terms of the generalized Laguerre polynomials $L_n^{\,k}(x) = \frac{e^x x^{-k}}{n!} \frac{d^n}{dx^n}(e^{-x} x^{n+k})$ (Auvil and Brown, 1978) and using Equation (2) we have

$$R(s) = B_n s^{[1+(1-c')^{1/2}]} \exp[-(-A')^{1/2} s] n! L_n^{\,k}(2(-A')^{1/2} s) \quad (29)$$

By using $U(s) = rR(s)$ we find

$$U(r) = Nr[1 - \exp(-2\alpha r)]^{[1+(1-c')^{1/2}]} \exp[-(-A')^{1/2}(1 - \exp(-2\alpha r))] n! L_n^{\,k} \quad (30)$$

Where N is the normalization constant. We have obtained the energy eigenvalues and the wave function of the radial K-G equation for modified Eckart potential plus Hulthen potential with scalar and vector potential for l≠0.

A SOME SPECIAL CASES

Here, we consider some special cases of interest if we consider spatially independent mass and spin symmetry we have

$$M(r) = m_0, \; m_1 = m_2 = 0 \quad (31)$$

$$V(r) = S(r), \; v_0 = s_0 \quad (32)$$

We have from Equation (19a) and (19b) the following equations.

$$A'' = E^2 + 2E - \gamma', \; \gamma' = m_0(m_0 + 1)$$
$$B'' = a'E + b', \; a' = -2(v_0 + 2), \; b' = -2m_0(v_0 + 2) \quad (33)$$

$$C'' = -4\alpha^2 \ell(\ell + 1)$$

And we have energy eigenvalues by

$$E_{n,\ell} = \frac{-(4m_0(2+v_0)^2 + \alpha') \pm \alpha'(m_0 - 1)}{4(2+v_0)^2 + \alpha'},$$
$$\alpha' = [(2n+1) + 2(1-C'')^{1/2}]^2 \quad (34)$$

Thus, the wave function can be written as,

$$U(r) = Nr[1 - \exp(-2\alpha r)]^{[1+(1-c')^{1/2}]} \exp[-(-A'')^{1/2}(1 - \exp(-2\alpha r))] n! L_n^{\,k} \quad (35)$$

We have obtained the energy eigenvalues and the wave function of the radial K-G equation for independent mass and spin symmetry for l≠0.

CONCLUSIONS

In this paper, we have discussed approximately the solutions of the Klein - Gordon equation for modified Eckart potential plus Hulthen potential with scalar and vector potential for l≠0 and position-dependent mass. We can obtain the energy eigenvalues and the wave function in terms of the generalized Laguerre polynomials functions via the Nikiforov-Uvarov method. We have also considered the limiting cases of spin symmetry and position-independent mass to obtain the energy eigenvalues and the wave function. We can conclude that our results are interesting for experimental physicists, because the results are exact, more general and useful to study nuclear scattering, nuclear and particle physics.

Conflict of Interest

The authors have not declared any conflict of interest.

REFERENCES

Alberto P, de Castro AS, Malheiro M (2013). Spin and pseudospin symmetries of the Dirac equation with confining central potentials. Phys. Rev. C 87, 031301(R).

Alhaidari AD (2001). Relativistic extension of shape-invariant potentials, J. Phys. A: Math. Gen. 34:9827.

Antia AD, ikot AN, Ituen EE, Akpan IO (2012). Bound state solutions of the Klein - Gordon equation for deformed Hulthen potential with position dependent mass. S. Lankan. J. Phys. 13(1):27-40.

ARDA A, Sever R, Tezcan C (2009). Approximate Analytical Solutions of the Klein-Gordon Equation for the Hulthen Potential with Position-Dependent Mass. Phys. Scr. 79:015006.

Arda A, Sever R, Tezcan C (2010). Analytical Solutions to the Klein–Gordon Equation with Position-Dependent Mass for q-Parameter Pöschl–Teller Potential. Chin. Phys. Lett.27:010306.

Arias de Saavedra F, Boronat J, Polls A, Fabrocini A (1994). Effective mass of one He4 atom in liquid He_3. Phys. Rev. B. 50: 4248(R).

Astorga AC, Andez DJ, Negro J (2012). Solutions of the Dirac Equation in a Magnetic Field and Intertwining Operators. SIGMA. 8:082.

AUVIL PR, BROWN LM (1978). The relativistic hydrogen atom: A simple solution. Am. J. Phys. 46(6):679-681.

Aygun M, Boztosun D, Sahin Y (2012). Solution of the Klein-Gordon Equation with Position-Dependent Mass for Exponential Scalar and Vector Potentials by an Alternative Approach. GU. J. Sci. 25(2):317-321.

Barranco M, Pi M, Gatica SM, Hernandez ES, Navarro J (1997). Structure and energetics of mixed 4He-3He drops. Phys. Rev. B. 56:8997.

Berkdemir C, Berkdemir A, Sever R (2006). Systematical approach to the exact solution of the Dirac equation for a deformed form of the Woods–Saxon potential. Phys. A: Math. Gen. 399:13455.

Berkdemir C, Berkdemir A, Sever R (2006). Systematical approach to the exact solution of the Dirac equation for a deformed form of the Woods-Saxon potential. J. Phys. A: Math. Gen. 39(43):13455.

Chen CY (2005). Exact solutions of the Dirac equation with scalar and vector Hartmann potentials. Phys. Lett. A. 339:283-287.

Cheng YF, Dai TQ (2007). Exact solution of the Schrödinger equation for the modified Kratzer potential plus a ring-shaped potential by the Nikiforov–Uvarov method. Phys. Scr.75:274.

Cheng YF, Dai TQ (2007). Exact Solutions of the Klein-Gordon Equation with a Ring-shaped Modified Kratzer Potential. Chin. J. Phys. 45:480.

Ciftci H, Hall RL, Saad N (2003). Asymptotic iteration method for eigenvalue problems. J. Phys. A. 36:11807.

de Souza Dutra A, Hott M (2006). Dirac equation exact solutions for generalized asymmetrical Hartmann potentials. Phys. Lett. A. 356:215-219.

Farrokh M, Shojaeia MR, Rajabi AA (2013). Klein-Gordon equation with Hulth'en potential and position-dependent mass. Eur. Phys. J. Plus. 128:14.

Feizi H, Rajabi AA, Shojaei MR (2011). Supersymmetric Solution Of The Schrödinger Equation For Woods–Saxon Potential By Using The Pekeris Approximation. Acta Phys. Polonica B. 42:2143.

Feizi H, Shojaei MR, Rajabi AA (2013). Relativistic symmetries of the Manning-Rosen potential in the frame of supersymmetry. Eur. Phys. J. Plus 128:3.

Geller MR, Kohn W (1993). Quantum mechanics of electrons in crystals with graded composition. Phys. Rev. Lett. 70:3103.

Ginocchio JN (2005). Relativistic symmetries in nuclei and hadrons. Phys. Rep. 414:165.

Greiner W (2000). Relativistic Quantum Mechanics: Wave Equations (Springer, 2000).

Guo JY, Sheng ZQ (2005). Solution of the Dirac equation for the Woods–Saxon potential with spin and pseudospin symmetry. Phys. Lett. A. 338:90-96.

Hill EH (1954). The Theory of Vector Spherical Harmonics. Am. J. Phys. 22:211.

Ikot AN, Udoimuk AB, Akpabio LE (2011). Bound states solution of Klein-Gordon Equation with type - I equal vector and Scalar Poschl-Teller potential for Arbitray l – State. Am. J. Sci. Ind. Res. 2:179-183.

Jia CS, de Souza Dutra A (2006). Position-dependent effective mass Dirac equations with PT-symmetric and non-PT-symmetric potentials. J. Phys. A. Math. Gen. 39:11877.

Jia CS, Gao P, Peng XL (2006). Exact solution of the Dirac–Eckart problem with spin and pseudospin symmetry. J. Phys. A: Math. Gen. 39:7737.

Jia CS, Li XP, Zhang LH (2012). Exact Solutions of the Klein–Gordon Equation with Position-Dependent Mass for Mixed Vector and Scalar Kink-Like Potentials. Few-Body Syst. 52:11–18.

Landau LD, Lifshitz EM (1977). Quantum Mechanics, Non-Relativistic Theory, 3rd. Edition, Pergamon, Ox-ford.

O¨ ZER O, LE´VAI G (2012). Asymptotic Iteration Method Applied To Bound-State Problems With Unbroken And Broken Supersymmetry. Rom. J. Phys. 57(3-4):582–593.

Oyewumi KJ, Akoshile CO (2010). Bound state solutions of the Dirac-Rosen-Morse potential with spin and pseudospin symmetry. Eur. Phys. J. A. 45:311-318.

Qiang WC (2003). Bound states of the Klein-Gordon and Dirac equations for potential $V(r) = Ar^{-2}-Br^{-1}$. Chin. Phys. 12(10):1054.

Qiang WC (2004). Bound states of the Klein–Gordon equation for ring-shaped Kratzer-type potential. Chin. Phys. 13:575.

Rajabi AA, Hamzavi M (2013). A new Coulomb ring-shaped potential via generalized parametric Nikiforov-Uvarov method. Int. J. Theor. Phys. 7(7):17.

Schiff LI (1955). Quantum Mechanics, 3rd Edition,McGraw-Hill, New York.

Serra L, Lipparini E (1997). Spin response of unpolarized quantum dots phys. Euro. Lett. 40:667.

Shojaei MR, Rajabi AA, Farrokh M, Zoghi-Foumani N (2014). Energy Levels of Spin-1/2 Particles with Yukawa Interaction. Int. J. Mod. Phys. 5:773-780.

VonRoos O (1983). Position-dependent effective masses in semiconductor theory. Phys. Rev. B. 27:7547.

Xue-Cai Z, Quan-Wen L, Chun-Sheng J, Li-Zhi W (2005). Bound states of the Dirac equation with vector and scalar Scarf-type potentials. Phys. Lett. A. 340:59-69.

Yi LZ, Diao YF, Liu JY, Jia CS (2004). Bound states of the Klein–Gordon equation with vector and scalar Rosen–Morse-type potentials. Phys. Lett. A. 333:212-217.

Zhang XC, Liu QW, Jia CS, Wang LZ (2005). Bound states of the Dirac equation with vector and scalar Scarf-type potentials. Phys. Lett. A. 340:59

International Journal of Physical Sciences

Related Journals Published by Academic Journals

- *African Journal of Pure and Applied Chemistry*
- *Journal of Internet and Information Systems*
- *Journal of Geology and Mining Research*
- *Journal of Oceanography and Marine Science*
- *Journal of Environmental Chemistry and Ecotoxicology*
- *Journal of Petroleum Technology and Alternative Fuels*

academicJournals